ATOMIC SCALE IMAGING AND CHARACTERIZATION OF ELECTRONIC DEFECT STATES IN DIELECTRIC THIN FILM MATERIALS USING DYNAMIC TUNNELING FORCE MICROSCOPY

by

Ruiyao Wang

A dissertation submitted to the faculty of
The University of Utah
in partial fulfillment of the requirements for the degree of

Doctor of Philosophy

in

Physics

Department of Physics and Astronomy

The University of Utah

August 2015

The University of Utah Graduate School

STATEMENT OF DISSERTATION APPROVAL

The dissertation of **Ruiyao Wang**

has been approved by the following supervisory committee members:

Clayton C. Williams	, Chair	**4/24/2015**
		Date Approved
Eugene Mishchenko	, Member	**4/24/2015**
		Date Approved
Stephan LeBohec	, Member	**4/24/2015**
		Date Approved
Michael Vershinin	, Member	**4/24/2015**
		Date Approved
Henry S. White	, Member	**4/24/2015**
		Date Approved

and by **Carleton DeTar**, Chair/Dean of

the Department/College/School of **Physics and Astronomy**

and by David B. Kieda, Dean of The Graduate School.

ABSTRACT

Dynamic Tunneling Force Microscopy (DTFM) is an Atomic Force Microscopy (AFM) technique used for imaging and characterizing trap states on nonconducting surfaces. In this thesis, DTFM images are acquired under Kelvin Probe Force Microscopy (KPFM) feedback and height feedback control. Simultaneous acquisition of DTFM, surface potential, and topographic images is realized, and correlation between trap states, surface potential, and surface topography can be extracted. The methodology for obtaining three-dimensional location and energy of individual atomic scale electronic trap states is described. The energy and depth of states accessible by a DTFM experiment are calculated using tunneling and electrostatic models. The DTFM signal amplitude is derived using a one-dimensional electrostatic model. Comparison between simulated DTFM signal and experimental results show a good consistency, verifying the single electron tunneling model.

DTFM is demonstrated on interlayer dielectric materials. Density, spatial distribution, energy, and depth distribution of trap states in these materials are measured by DTFM. An atomic scale study of electrical stressing effects using the DTFM method is performed showing both state appearance and disappearance after electrical stressing.

CONTENTS

LIST OF FIGURES

Figures

ACKNOWLEDGMENTS

I'd like to thank Prof. Clayton Williams for allowing me to work on this project. Dr. Philipp Rahe has mentored me on instrumentation and physics, especially AFM knowledge. I owe many thanks to his selfless help. Adam Payne trained me on UHV AFM. My sincere thanks also go to Kapildeb Ambal and Dr. Dustin Winslow for their help in my work.

CHAPTER 1

INTRODUCTION

1.1 Motivation and Objectives

Interlayer dielectric (ILD) films are very important components in ultra large scale integrated circuit (ULSI) as they decouple signals between lines. Electrical reliability has always been a focus of the study of those materials. Defect states play an essential role in film leakage and breakdown [1-3], and thus characterization of those defect states will be illuminating for material reliability issues. Those states have been probed using macroscopic methods [4-10], but those methods can only provide information on ensemble of states. As semiconductor devices shrink to single digit nanometer dimensions, atomic scale understanding of individual defect states is very important [11]. Dynamic tunneling force microscopy (DTFM) [12], previously developed in Prof. Williams' group, is a scanning probe microscopy (SPM) method that can image three-dimensional locations of trap states at atomic scale on nonconducting surface. In this thesis, volume density, energy, and depth of trap states in ILD films are characterized using DTFM.

1.2 Trap States in Interlayer Dielectric (ILD) Films

Novel materials are developed to replace SiO_2 for different purposes. For example, low-k interlayer dielectrics (ILD) [13] have been used to reduce the capacitance between

metal lines, therefore increasing the circuit speed as device size scales down. Lower k is achieved by incorporating pores or low polarizability bonds. The samples used in this study are silicon oxide doped with carbon, hydrogen, and/or nitrogen at various ratios. Some of the samples are porous.

Electrical reliability of those ILD materials is closely correlated with trap states. Current-voltage (I-V) measurements on ILD films similar as measured in this thesis research indicate that several conduction mechanisms dominate at different electrical field ranges [1]. Poole-Frenkel emission is most commonly observed as the dominant leakage mechanism at moderate to high electrical fields [1,2,14,15]. Poole-Frenkel emission is due to electrical field enhanced thermal excitation of trapped electrons into conduction band of dielectric [16]. The energetic depth of the trap states below conduction band is the barrier height for the thermal excitation. Trap-assisted Fowler-Nordheim tunneling is also argued to be a conduction mechanism of dielectric films at high electrical field [3]. In this case, electrons in the trap states tunnel into conduction band by Fowler-Nordheim tunneling [16]. At lower electrical fields, conduction of those films is related to electron hopping between trap states [1,2]. Additionally, generation of electron traps by electrical stress has been proposed as a cause of SiO_2 breakdown [17-20]. Electron trap state density is also correlated with increase in leakage current during electric stress [2]. Therefore, trap states have been shown to play a vital role in film leakage, degradation, and breakdown. Investigation of those trap states in ILD films will shed light on the electrical properties of those materials and eventually help to improve device performance.

Much work has been done to characterize electron states in ILD films using

macroscopic material characterization methods. For example, paramagnetic defect densities have been measured using electron spin resonance (ESR) [4,5] and electrically detected magnetic resonance (EDMR) [6]. Trap state density at the Si/ILD interface with a faster rate of filling and emptying than bulk state can be measured by conductance and capacitance techniques [7]. De-trapping current following photoexcitation [8,9] and photoinduced I-V measurements [8] are also utilized to measure trap density. Kelvin Probe [9] and capacitance-voltage curves [9,10] measure trapped charge in the dielectric. The defects can be linked to chemical bonding structure using Fourier transform infrared (FTIR) spectroscopy [4]. While those macroscopic methods provide powerful means in characterizing electron states in ILD materials, they do not have enough spatial resolution to probe individual states at the atomic level, which is important for the understanding of the defects and also for its relevance to single electron device concept as semiconductor device size continues to scale down. For this purpose, scanning probe microscopy (SPM) can be a powerful tool.

1.3 Related Scanning Probe Microscopy Techniques for Probing Electronic States in Nonconducting Surfaces

Starting from the Nobel Prize winning invention of Scanning Tunneling Microscope (STM) in 1981, scanning probe microscopy (SPM) has rapidly developed into a large technique family in surface science providing powerful means of investigating various properties of the surface at atomic scale. In SPM, a physical probe is brought into proximity of the surface generally realized by using a feedback loop operating on some interaction between the tip and sample, e.g. tunneling current or atomic force. One or multiple of these interactions between SPM tip and the surface are

measured and recorded as a function of surface locations during imaging. Among a vast variety of SPM methods, only a few are reviewed here, which can characterize electronic states on nonconducting surfaces.

By inducing a current flow through a dielectric film, a thin dielectric film can be characterized using Scanning Tunneling Microscope (STM) [21,22], ballistic electron microscopy (BEEM) [23], and conductive Atomic Force Microscopy (c-AFM) [24-26]. In STM [27], electrons tunnel through the gap between tip and surface, and the resultant current is used as height feedback control signal. Benefitting from the exponential decay of tunneling current with respect to tunneling gap--approximately one order of magnitude increase of current as the tip is moved one Angstrom closer to the surface, STM can achieve atomic resolution because only the very end of the tip apex participates in tunneling. Trapping of a single electron by a defect state in SiO_2 can induce a detectable change in tunneling current nearby; therefore, trap states can be detected by STM [21,22]. BEEM [28,29] combines measurement of STM current to a surface metal layer and collection of ballistic electron flux (BEEM current) through the oxide underneath the metal surface to probe trap states in the oxide [23]. c-AFM is an atomic force microscopy (AFM) method using atomic force between tip and surface as the tip height feedback control, while current through the oxide is measured in another channel. c-AFM is more appropriate for studying dielectric surfaces than STM because it does not rely on a measurable current to control tip height during imaging and it also separates current information from topographical information. Current measured in c-AFM through an oxide film is often due to electrons injected from tip or substrate (depending on the polarity of applied voltage) into the dielectric conduction band through Fowler-Nordheim

tunneling [24-26]. Therefore, I-V curves can be used to extract the tunneling barrier height and oxide thickness. High current locations measured in c-AFM imaging could be an indication of defect states which provide a current path or reduced tunneling barrier. For all of these three SPM methods, which measure current, adequate conductivity of the dielectric film is required for a detectable current in the order of 0.1pA (10^6 electrons/second). Those methods do not work on completely nonconducting films.

Electrostatic force microscopy (EFM) [30] detects the electrostatic force on the tip caused by the charge at the sample surface. The sensitivity of the EFM to surface charge depends on system noise. In our system, less than 1/10 of a single electron charge can be easily detected [31]. Kelvin probe force microscopy (KPFM) [32] applies a voltage modulation between tip and surface, and the surface potential is detected by a lock-in amplifier. Notice that EFM and KPFM can only measure charged trapping sites in the surface rather than neutral states. Atomic scale scanning capacitance microscopy (SCM) [33] imaging has not been achieved due to either probe tip size or limited sensitivity.

1.4 Detection of Trap States on Dielectric Surfaces by Single Electron Tunneling – Background Work

In the Williams' lab, isolated electronic states in dielectric surfaces are detected by single electron tunneling between a metal tip and the state. This technique was first demonstrated using amplitude detection electrostatic force microscopy (EFM) [34]. Amplitude detection EFM was replaced later by frequency detection EFM [31], which continues to be used to the present time. A sudden change in resonance frequency shift (df) is observed when an electron tunnels between tip and sample. The amplitude of the

measured df change agrees with single electron tunneling theory, as predicted by an electrostatic model [31], and the tip/surface gap is consistent with the barrier width at which tunneling may occur by a tunneling model [35]. Therefore, the abrupt df change is explained as a single electron tunneling event between the tip and a trap state in oxide surface. Energy of the state can be obtained by measuring the resonance frequency shift of the probe as a function of voltage applied between the probe and the surface back-contact (df-V curve) [36]. Tunneling -- observed as an abrupt change in df in otherwise smooth df-V curve -- is triggered when the tip Fermi level moves across the energy level of the state. To image the trap states in 2D, single-electron tunneling force microscopy [37] was developed based upon depositing and extracting electrons through tunneling to trap states by quasi-statically varying tip height and applied voltage and detecting the surface potential change at each point as the tip is scanned across the surface. This method was later replaced by dynamic tunneling force microscopy (DTFM), which dynamically tunnels an electron between the tip and the surface state and detects the shuttling charge caused df modulation [12]. Work in this thesis improves the DTFM method in experimental design, fully simulates the DTFM signal and compares it with experimental data, develops a methodology to measure three-dimensional location and energy of individual trap states using DTFM, and applies the method to several different dielectric films.

In this section, the electrostatic model for charge detection and the tunneling model for a metal tip and a trap state in the surface are reviewed. These two models provide the theoretical foundation for the trap state detection by single electron tunneling techniques developed in the Williams' group.

1.4.1 Detection of charge in dielectric surface by electrostatic force

Charge detection in frequency modulated EFM is based on force detection by noncontact atomic force microscopy (NC-AFM). Figure 1.1 is the schematic of the typical EFM experiment apparatus. A focused laser beam is incident on the back of an oscillating AFM probe and reflected to a photodiode. The laser deflection signal goes through a phase locked loop (PLL) used as the FM demodulator. The tip oscillation amplitude is kept constant by a feedback loop. In constant oscillation amplitude mode, the cantilever oscillating frequency shift (df) away from its resonance frequency (f_0) is caused by the force gradient on the tip. df change caused by surface charge in EFM is derived as following. In NC-AFM, an oscillating cantilever can be modeled as a driven, damped harmonic oscillator governed by the equation of motion [38]:

$$m^*\ddot{z} + \frac{k}{Q\omega_0}\dot{z} + kz = F_d\,, \tag{1.1}$$

where m^* is the effective mass of the cantilever, k is the cantilever stiffness, Q is the quality factor of the cantilever, ω_0 is the resonant frequency of the cantilever, z is the vertical position of the tip, and F_d is the driving force. If F_d is applied by a feedback loop to compensate for the cantilever damping and keep the oscillation amplitude fixed at a, (1.1) becomes

$$m^*\ddot{z} + kz = 0\,, \tag{1.2}$$

$$z = a\cos(\omega_0 t). \tag{1.3}$$

When the tip is brought close enough to the surface that it starts to feel an interaction force from the surface F(z), cantilever equations of motion become:

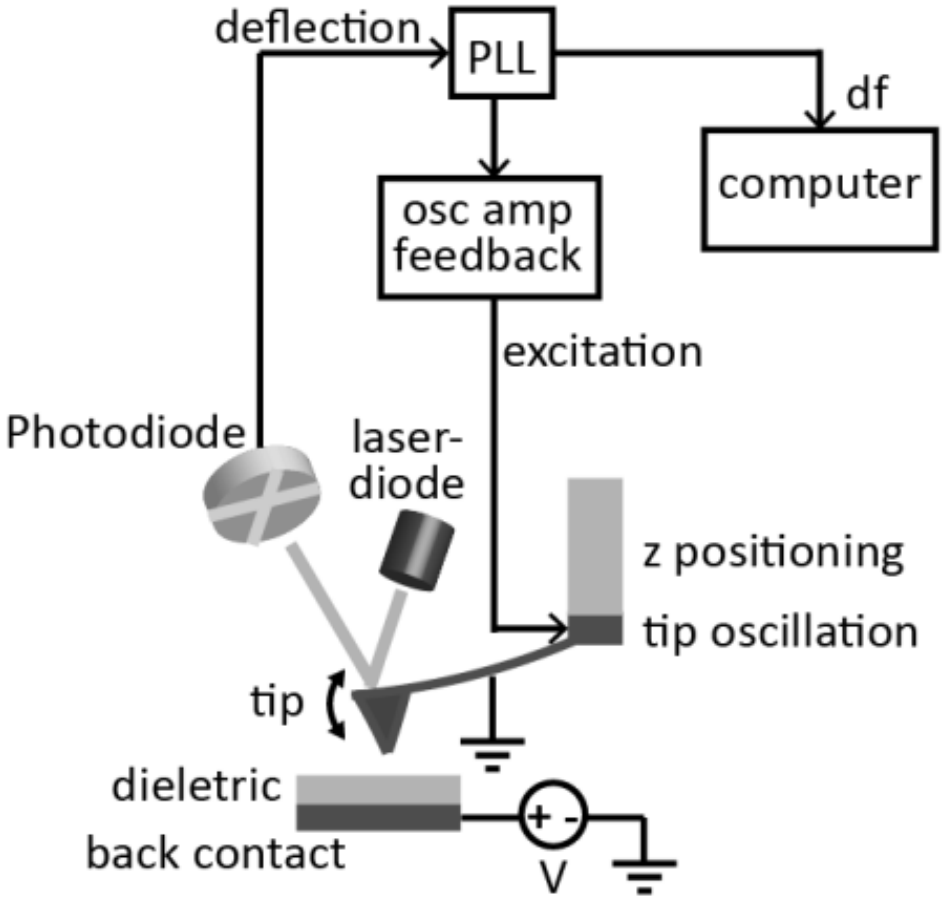

Figure 1.1 Schematic for frequency detection electrostatic force microscopy. A phase locked loop (PLL) demodulates laser deflection signal of an oscillating AFM tip, measuring the cantilever resonance frequency shift, df, caused by the electrostatic force gradient on the tip. The tip oscillation amplitude is kept constant by a feedback loop. In EFM, a voltage is often applied between the tip and the film back-contact.

$$m^*\ddot{z} + kz = F, \tag{1.4}$$

$$z = a\cos(\omega t). \tag{1.5}$$

The cantilever resonance frequency shifts to ω because of the external force gradient. The frequency shift $\Delta\omega = \omega - \omega_0$ is a measure of the tip/surface interaction. Insert (1.5) into (1.4) and we get

$$(\omega^2 - \omega_0^2)\cos(\omega t) = -\frac{\omega_0^2}{ak}F. \tag{1.6}$$

Under experiment conditions, $\omega_0 \gg \Delta\omega$. An approximation is made that $\omega^2 \cong \omega_0^2 + 2\omega_0\Delta\omega$, and (1.6) becomes

$$2\Delta\omega\cos(\omega t) = -\frac{\omega_0}{ak}F. \tag{1.7}$$

Replacing ω by $\omega_0$in $\cos(\omega t)$, multiply both sides of equation (1.7) by $\cos(\omega t)$, and then integrate both sides over a cantilever oscillation cycle. The mean frequency shift df is calculated to be [39]

$$df = \frac{f_0^2}{ka}\int_0^{1/f_0} F(z)cos(2\pi f_0 t)dt. \tag{1.8}$$

1.4.2 Tunneling between a metal tip and a trap state in dielectric surface

The elastic tunneling of an electron to a state in a dielectric film provides a way to probe the properties of that state, such as its energy and depth, and possibly even its chemical identity. This section reviews the conditions under which tunneling could occur between a metallic probe and a trap state in the dielectric film.

The first condition is the occupancy of the states at given energy levels. If an empty trap state in the dielectric is located below the tip Fermi level (or a filled state is located above the tip Fermi level), an electron will tunnel into the empty state (or out of the filled state) in the dielectric from (or into) the tip if the tunneling probability is high enough. Experimentally, the tip Fermi level is modulated relative to states in the sample by applying a voltage between tip and sample. By doing this, one can alternatively empty a state at one voltage polarity and fill it at the other, achieving single electron manipulation between tip and surface [40]. If we know the threshold voltage at which tunneling changes directions, the energy of the state can be deduced from that voltage using a simple one-dimensional (1D) electrostatic model [36].

The second condition for tunneling to occur is that the tunneling rate between tip and state in dielectric surface must be finite. The tunneling rate between tip and the state is determined by the quantum mechanical tunneling barrier width and height. The tunneling barrier width includes the barrier in the gap and in the dielectric film for those states at a finite depth. The barrier height depends on the energy level of the state with respect to vacuum level and dielectric conduction band. A state that is energetically shallower but physically deeper under the surface could have the same tunneling rate as a state that is energetically deeper but closer to the surface. A df-z curve [31] measures the threshold tip/surface gap at which tunneling rate becomes detectable in the experimental period.

When both of the two conditions above are met, an electron may tunnel to/from the state in the dielectric surface. The change of surface charge causes by an electron produces a change in electrostatic force on the tip, which is detected as a cantilever

frequency shift (df).

1.5 References

[1] K. Y. Yiang, W. J. Yoo, Q. Guo, and A. Krishnamoorthy, Appl. Phys. Lett. 83, 524 (2003).

[2] J. M. Atkin, T. M. Shaw, E. Liniger, R. B. Laibowitz, and T. F. Heinz, Reliability Physics Symposium (IRPS), 2012 IEEE International, pp. BD-1. IEEE, 2012.

[3] G. G. Gischia, K. Croes, G. Groeseneken, Z. Tokei, V. Afanas' ev, and L. Zhao, Reliability Physics Symposium (IRPS), 2010 IEEE International, pp. 549-555. IEEE, 2010.

[4] H. Ren, M. T. Nichols, G. Jiang, G. A. Antonelli, Y. Nishi, and J. L. Shohet, Appl. Phys. Lett. 98, 102903 (2011).

[5] B. C. Bittel, P. M. Lenahan, and S. W. King, Appl. Phys. Lett. 97, 063506 (2010).

[6] C. J. Cochrane and P. M. Lenahan, Appl. Phys. Lett. 104, 093503 (2014).

[7] J. M. Atkin, E. Cartier, T. M. Shaw, R. B. Laibowitz, and T. F. Heinz, Appl. Phys. Lett. 93, 122902 (2008).

[8] J. M. Atkin, D. Song, T. M. Shaw, E. Cartier, R. B. Laibowitz, and T. F. Heinz, J. Appl. Phys. 103, 094104 (2008).

[9] H. Sinha, H. Ren, M. T. Nichols, J. L. Lauer, M. Tomoyasu, N. M. Russell, G. Jiang, G. A. Antonelli, N. C. Fuller, S. U. Engelmann, Q. Lin, V. Ryan, Y. Nishi, and J. L. Shohet, J. Appl. Phys. 112, 111101 (2012).

[10] H. Sinha, J. L. Lauer, M. T. Nichols, G. A. Antonelli, Y. Nishi and J. L. Shohet, Appl. Phys. Lett. 96, 052901 (2010)

[11] S. King, H. Simka, D. Herr, H. Akinaga, and M. Garner, APL Mater. 1, 40701 (2013).

[12] J. P. Johnson, N. Zheng, and C. C. Williams, Nanotechnology 20, 055701 (2009).

[13] K. Maex, M. R. Baklanov, Denis Shamiryan, S. H. Brongersma, and Z. S. Yanovitskaya, J. Appl. Phys. 93, 8793 (2003).

[14] M. Vilmay, D. Roy, F. Volpi, and J. Chaix, Microelectron. Eng. 85, 2075 (2008).

[15] Y. Li , G. Groeseneken , K. Maex and Z. Tokei "Real-time investigation of conduction mechanism with bias stress in silica-based intermetal dielectrics", IEEE Trans. Device Mater. Rel., vol. 7, no. 2, pp.252 -258 2007

[16] S. M. Sze, Physics of Semiconductor Devices, 2nd ed. (Wiley, New York, 1981).

[17] E. Harari, J. Appl. Phys. 49, 2478 (1978).

[18] Y. Nissan-Cohen, J. Shappir, and D. Frohman-Bentchkowsky, J. Appl. Phys. 60, 2024 (1986).

[19] D. J. DiMaria and J. W. Stasiak, J. Appl. Phys. 65, 2342 (1989).

[20] S. Lombardo, J. H. Stathis, B. P. Linder, K. L. Pey, F. Palumbo, and C. H. Tung, J. Appl. Phys. 98, 121301 (2005).

[21] M. E. Welland and R. H. Koch, Appl. Phys. Lett. 48, 724 (1986).

[22] H. Watanabe, K. Fujita, and M. Ichikawa, Appl. Phys. Lett. 72, 1987 (1998).

[23] B. Kaczer, Z. Meng, and J. P. Pelz, Phys. Rev. Lett. 77, 91 (1996).

[24] T. Ruskell, R. Workman, D. Chen, D. Sarid, S. Dahl, and S. Gilbert, Appl. Phys. Lett. 68, 93 (1996).

[25] A. Olbrich, B. Ebersberger, and C. Boit, Appl. Phys. Lett. 73, 3114 (1998).

[26] M. Porti, M. Nafría, X. Aymerich, A. Olbrich, and B. Ebersberger, J. Appl. Phys. 91, 2071 (2002).

[27] G. Binnig, H. Rohrer, Ch. Gerber, and E. Weibel, Phys. Rev. Lett. 49, 57 (1982).

[28] W. J. Kaiser and L. D. Bell, Phys. Rev. Lett. 60, 1406 (1988)

[29] L. D. Bell and W. J. Kaiser, Phys. Rev. Lett. 61, 2368 (1988).

[30] P. Girard, Nanotechnology 12, 485 (2001).

[31] E. Bussmann, D. J. Kim, and C. C. Williams, Appl. Phys. Lett. 85, 2538 (2004).

[32] W. Melitz, J. Shen, A. C. Kummel, and S. Lee, Surf. Sci. Rep. 66, 1 (2011).

[33] Y. Naitou, H. Arimura, N. Kitano, S. Horie, T. Minami, M. Kosuda, H. Ogiso, T. Hosoi, T. Shimura, and H. Watanabe, Appl. Phys. Lett. 92, 012112 (2008).

[34] L. J. Klein and C. C. Williams, Appl. Phys. Lett. 81, 4589 (2002).

[35] Zheng N, Williams C C, Mishchenko E G and Bussmann E 2007 *J. Appl. Phys.* 101 093702

[36] E. Bussmann and C. C. Williams, Appl. Phys. Lett. 88, 263108 (2006).

[37] Bussmann E B, Zheng N and Williams C C 2006 *Nano Lett.* 6 2577.

[38] D. Sarid, Scanning Force Microscopy with Applications to Electric, Magnetic, and Atomic Forces (Oxford University Press, New York, 1994).

[39] F. J. Giessibl, Appl. Phys. Lett. 78, 123 (2001).

[40] E. Bussmann, N. Zheng, and C. C. Williams, Appl. Phys. Lett. 86, 163109 (2005).

CHAPTER 2

ATOMIC SCALE TRAP STATE CHARACTERIZATION BY DYNAMIC TUNNELING FORCE MICROSCOPY

This chapter contains a paper that was published in Applied Physics Letters **105**, 052903 (2014) entitled Atomic Scale Trap State Characterization by Dynamic Tunneling Force Microscopy by R. Wang, S. W. King, and C. C. Williams.[1] It contains first DTFM imaging results under surface potential and height feedbacks and demonstrates energy/depth extraction for individual trap states in low-k dielectrics from DTFM images. The paper has been reformatted to match the style of this dissertation.

2.1 Abstract

Dynamic tunneling force microscopy (DTFM) is applied to the study of point defects in an inter-layer dielectric film. A recent development enables simultaneous acquisition of DTFM, surface potential and topographic images while under active height feedback control. The images show no clear correlation between trap state location and surface potential or topography of the surface. The energy and depth of individual trap states are determined by DTFM images obtained at different probe tip heights and applied voltages and quantitative tunneling and electrostatic models. The measured density of states in these films is found to be approximately 1×10^{19} cm^{-3} eV^{-1} near the

[1] Reprinted with permission from Applied Physics Letters 105, 052903 (2014). Copyright 2014, American Institute of Physics.

dielectric film surface.

2.2 Paper Body

Electron trap states are found in dielectric materials and influence their electronic properties and performance in device structures [1]. For example, low-k inter-layer dielectric (ILD) films [2] are used to separate metal lines between electronic devices to ensure a high operational speed of the circuit. Reliability of these materials is a major concern, as electronic trap states play a role in film leakage and breakdown [3-5]. Significant work has been done in characterizing such defect states using electron spin resonance (ESR) [6,7], electrically detected magnetic resonance (EDMR) [8], conductance and capacitance techniques [9], and by measuring de-trapping current following photo-excitation [10, 11]. However, these macroscopic methods only probe the ensemble of trap states. As semiconductor devices march toward single digit nanometer dimensions, an atomic scale understanding of individual defect states and the role they play in these materials is needed [12].

Electrical properties of dielectric films have been characterized using scanning probe microscopy (SPM) methods, such as scanning tunneling microscopy (STM) [13], conductive atomic force microscopy (c-AFM) [14], ballistic electron emission microscopy (BEEM) [15], Kelvin probe force microscopy (KPFM) [16], electrostatic force microscopy (EFM) [17], and scanning capacitance microscopy (SCM) [18]. Among these, STM, c-AFM and BEEM are limited by the requirement that a detectable current must be achieved and therefore they apply only to dielectric films with adequate conductance. KPFM and EFM can only measure charged trapping sites rather than neutral states. Atomic scale SCM imaging has not been achieved due to either finite

probe tip radius or limited sensitivity.

Dynamic tunneling force microscopy (DTFM) [19] is based upon single electron tunneling between an AFM probe tip and a single trap state near the sample surface [20,21]. The electron tunneling is detected by the electrostatic force the charge produces on the probe tip, providing a method to detect and image electron trap states in completely non-conductive surfaces. The spatial resolution of the method benefits from the exponential dependence of tunneling rate with gap, as in Scanning Tunneling Microscopy, and therefore atomic scale imaging can be achieved. The first DTFM images were obtained using a constant probe height mode (no probe height feedback). To achieve high quality DTFM images, however, the tip-sample gap must be maintained constant to within a fraction of a nanometer during the acquisition of an image, which typically takes a few minutes. Reducing the tip-sample thermal drift and piezoelectric creep to a fraction of a nanometer per image is difficult and time consuming. Additionally, imaging in constant height mode does not work on surfaces that are not atomically flat. Operating with AFM probe height feedback eliminates both issues and allows images to be acquired over long time periods.

A method to provide height feedback control during DTFM imaging has been developed which facilitates acquisition of full images with a constant tip-sample gap. To achieve this, it is necessary to implement a Kelvin probe force microscopy (KPFM) feedback loop [22] to null the electrical field between tip and surface. This helps to keep the cantilever frequency shift (df) independent of surface potential variations, so that df can be used to keep the tip-sample gap constant. Keeping the tip at the same potential as the local surface also provides a useful reference for energy measurements, as described

below. Moreover, two additional channels of simultaneous information (surface potential and topography) are provided by the improved method. Correlation of the three independent channels provides additional physical understanding of the dielectric film and the trap states observed.

Figure 2.1 shows the DTFM experimental set-up. Measurements are performed with an Omicron Multiprobe S atomic force microscope under a vacuum of 10^{-10} mBar at room temperature. A metal coated AFM probe (NanosensorPPP-NCHPt), with ~10 nm tip oscillation amplitude and ~40 N/m stiffness is brought within tunneling range of a dielectric surface. A periodic asymmetric square wave shuttling voltage at ~300 Hz is applied to the sample with tip grounded, consisting of a positive voltage ($+V_{ac}$) for 77% of its duty cycle and a negative voltage ($-V_{ac}$) for the remaining 23%. The tip height is also modulated sinusoidally (z_{mod}) with a 2nm amplitude at twice the shuttling voltage frequency. Waveforms of voltage and height modulations are synchronized as shown in Figure 2.1. The cantilever frequency shift (df) signal goes to a two phase lock-in amplifier which is referenced with the shuttling voltage. The in-phase and quadrature phase components of the frequency shift (df) signal at 300 Hz are both measured. The in-phase component corresponds to the local surface potential of the sample, which is kept at zero via a KPFM feedback loop, and the quadrature phase component of df is the DTFM signal. The average frequency shift (df) is used to control tip height during scanning.

The DTFM method without height and KPFM feedback is explained in detail in Reference [19]. Briefly, the square wave shuttling voltage is applied to move the tip Fermi level between a high and a low level with respect to the trap states in the surface.

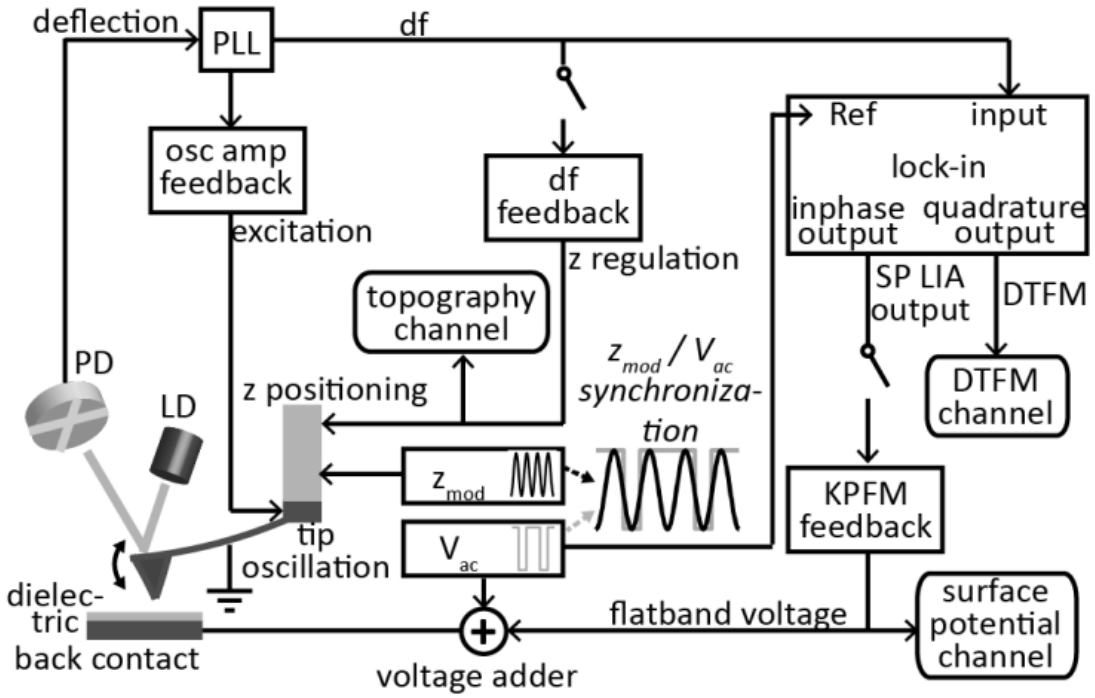

Figure 2.1 Block diagram of the DTFM method with height and Kelvin probe force microscopy feedback control. z_{mod} is a sinusoidal modulation applied to the probe tip height and V_{ac} is an asymmetric square wave voltage applied to the sample. Synchronization of the z_{mod} and V_{ac} are shown above. The in-phase output signal of the lock-in amplifier (with V_{ac} as reference) is denoted as the surface potential lock-in amplifier output (SP LIA output), to differentiate from surface potential signal, which in this paper denotes the KPFM feedback voltage applied to the sample (to keep the tip and sample at flat band). The photodiode, laser diode, phase lock loop, and oscillation amplitude are denoted as PD, LD, PLL, and osc amp.

This induces electrons to tunnel to and from these states. The height modulation is to bring the tip into and out of tunneling range. This causes the electron tunneling (shuttling) to occur with a phase that is approximately 90 degrees out of phase with surface potential signal. If a trap state is at a depth that is within tunneling range and also has an energy between the high and low tip Fermi level positions, an electron will shuttle between the tip and the state at the frequency of the shuttling voltage. This electron shuttling causes a periodic electrostatic force gradient on the probe, which is detected as a periodic frequency shift of the probe oscillation frequency. This frequency shift is detected by a lock-in amplifier in quadrature with the applied shuttling voltage.

The sample utilized in this study is a 6nm low-k ILD film (k=3.3) a-$SiO_{1.2}C_{0.35}$:H fabricated at Intel Corporation by plasma enhanced chemical vapor deposition (PECVD). Details concerning film deposition process can be found in Reference [23]. The sample was ultrasonically cleaned both in acetone and isopropyl alcohol for 15 minutes, then rinsed in deionized water and blown dry with nitrogen gas. The sample was then inserted in the UHV chamber and heated at 380^{o}C for 1 hour to desorb water and organic contaminants from ambient exposure.

DTFM images are acquired on a $(50nm)^2$ area of the ILD sample surface at various tip-surface gaps (z_{min}) and shuttling voltages (V_{ac}) (see Figure 2.2(a)-(h)). The tip-sample gap is determined by pulling the tip back a known distance from the position at which the df-z curve reaches a minimum value [21].

As the tip is scanned laterally across a trap state accessible by tunneling, an electron will shuttle between the tip and state and the DTFM signal increases. Each bright region in the DTFM image therefore represents an individual electron trap state. The

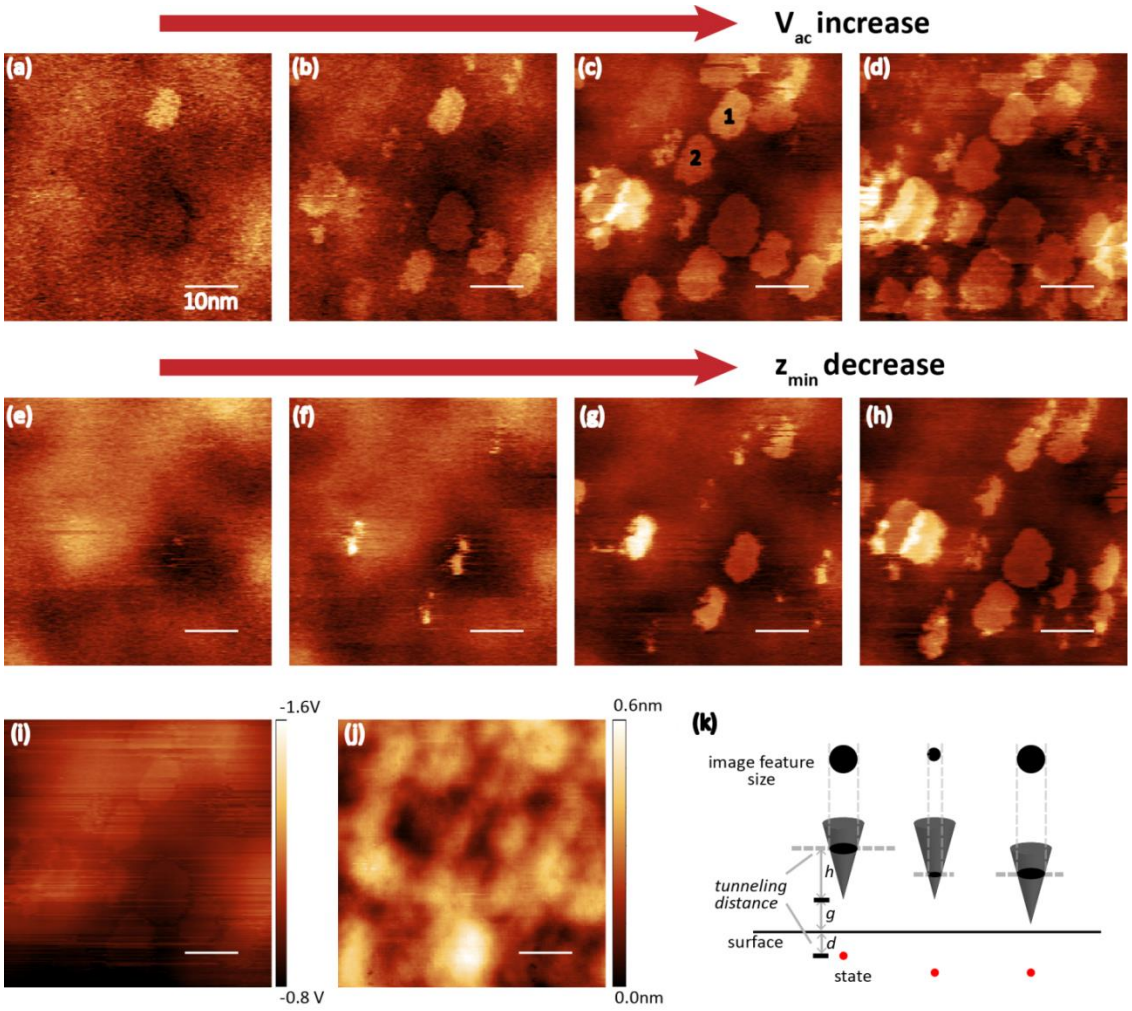

Figure 2.2 DTFM images taken at different V_{ac} and z_{min} on k=3.3 ILD sample. (a)-(h) are DTFM images taken in the same sample area at different tip-surface gaps (z_{min} is the smallest tip-sample gap during tip height modulation) and shuttling voltages (V_{ac}). The scale bar is 10nm in all images. (a) z_{min} = 0.5nm, V_{ac} = 0.5V (b) z_{min} = 0.5nm, V_{ac}= 1V (c) z_{min} = 0.5nm, V_{ac}= 2V (d) z_{min} = 0.5nm, V_{ac} = 3V (e) z_{min} = 1.3nm, V_{ac} = 3V (f) z_{min} = 1.1nm, V_{ac} = 3V (g) z_{min} =0.9nm, V_{ac} =3V (h) z_{min} =0.7nm, V_{ac} =3V. The color scale is chosen independently in each image for best contrast. Two particular states are identified by numbers 1 and 2 in (c). (i) is a surface potential image. (j) is a topography image. Both (i) and (j) are simultaneously acquired with the DTFM image (c). (k) illustrates the principle behind the apparent size of the trap states in the DTFM images. d is the trap state depth in the film, g is the tip-sample gap, and h is the height above the tip apex from which tunneling to a particular state can occur.

DTFM image is a two-dimensional map of the trap states accessible to tunneling in the dielectric surface. The apparent size of each bright region may be much larger than the true spatial extent of the trap states, as the size is determined by a tip imaging effect [19]. The apparent size of a given trap state is influenced by its depth, the tip height and the shape of the probe apex (see Figure 2(k)).

The surface potential image (Figure 2.2(i)) and topography image (Figure 2.2 (j)) in this sample region are simultaneously acquired with the DTFM image (Figure 2.2 (c)). Comparison of the DTFM, surface potential and topography images shows that there is little correlation between the trap state locations (bright spots in DTFM image) and local surface potential or topography. There is a slowly varying background observed in the DTFM image, which does appear to be correlated with the corresponding surface potential image. This correlation is currently under study. Note that there is also a weak DTFM-like signal which appears in the surface potential image at the trap state locations of DTFM image. This is due to the fact that when electron shuttling occurs, there is a small average surface potential shift caused by the additional average surface charge in the state (½ electron) due to the electron shuttling [24].

Figure 2.2 also shows a comparison between DTFM images at different tip-sample gaps (z_{min}) and applied voltages (V_{ac}). As V_{ac} increases (Figure 2.2(a)-(d)) at constant z_{min}, new states appear while the previously observed states remain. This can be explained by the fact that as V_{ac} is increased, a larger energy range of trap states are being accessed, due to the larger movement of the tip Fermi level. As z_{min} decreases (Figure 2.2(f)-(i)) at constant V_{ac}, more states appear because states deeper in the film are accessible to tunneling as tip moves closer to surface.

The energy and depth of trap states accessible by DTFM with a given V_{ac} and z_{min} are calculated using an electrostatic and tunneling model from Reference [25] (Figure 2.3). Some improvements have been made to more accurately account for tip motion [24]. The depth of the states accessible to tunneling is determined by the tunneling barrier, which includes the barrier in the gap and in the film, for those states at a finite depth. The barrier height in the film depends on the trap state energy. The energies accessible by tunneling are determined by the shuttling voltage (V_{ac}). Accessibility to tunneling is calculated numerically for a grid of points in energy/depth space for given z_{min} and V_{ac}. In the tunneling rate calculations [26], the following physical parameters have been used: electron effective mass (0.5 times electron mass in vacuum [27]), platinum tip work function (5.4eV [28]), platinum tip Fermi energy relative to bottom of band (8.5eV), dielectric film electron affinity (0.7eV [29]) and band gap (8.2eV [23]). The tip Fermi level under the flat band condition is assigned to be zero energy in Figure 2.3 and 2.4 (on left vertical axis), which is equivalent to 3.5eV above the dielectric valence band (right vertical axis of Figure 2.4). Since we actively keep the surface and tip at flat band during DTFM imaging, energies of the states can be determined unambiguously with respect to dielectric energy bands as long as band structure of the tip and dielectric are known. From Figure 2.3, we can see that as V_{ac} increases, more states in a larger energy range become accessible, and as z_{min} decreases, deeper states become accessible.

Each individual state observed in the images shown in Figure 2.2 can be assigned to a particular region of energy-depth space by differentially subtracting the regions calculated for different z_{min} and V_{ac} [25]. In Figure 2.4, each energy/depth region is

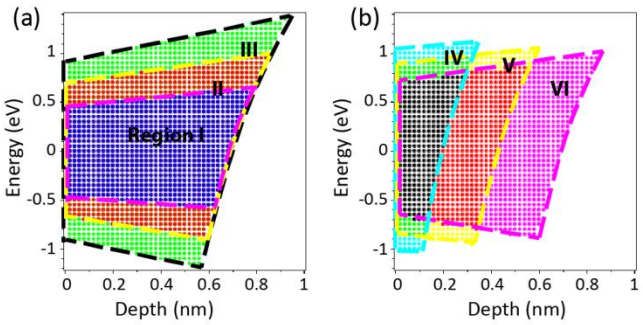

Figure 2.3 Calculated regions of energy and depth accessible by DTFM at different shuttling voltages and probe heights. Numerical calculation of tunneling probability leads to a grid of points showing tunneling accessible energies and depths. Approximate boundary lines are drawn to guide the eye. (a) Region I corresponds to a z_{min} = 0.5nm and V_{ac} = 2V, region II: z_{min} = 0.5nm and V_{ac} = 3V, and region III: z_{min} = 0.5nm and V_{ac} = 4V (b) Region IV: V_{ac} = 3V and z_{min} = 0.9nm, region V:V_{ac} = 3V and z_{min} 0.7nm, and region VI: V_{ac} = 3V and z_{min} = 0.5nm (same as region II in (a)).

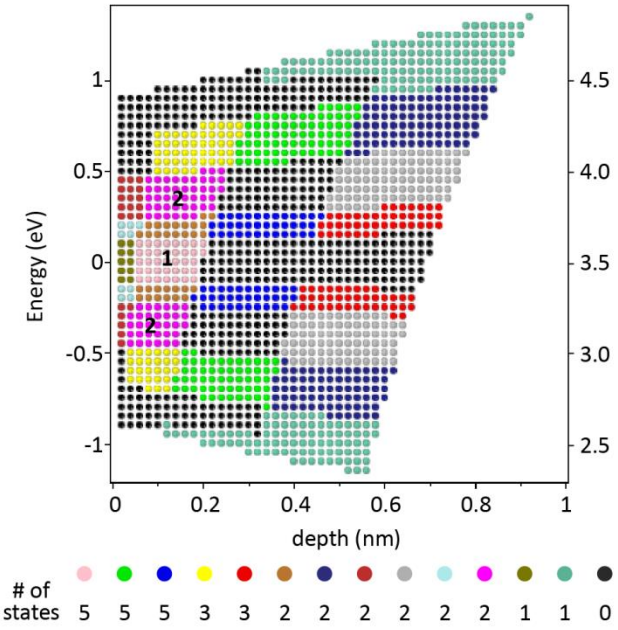

Figure 2.4 Differential energy-depth regions calculated for the states shown in the images of Figure 2.2. (Data from an additional DTFM image with z_{min} = 0.5nm, V_{ac}= 4V is not shown in Figure 2.2) The energy axis on the left is relative to tip Fermi level at flatband and the energy axis on the right is relative to dielectric valence mobility edge. State 1 and 2 identified in Figure 2.2(c) are found to fall into the pink and magenta energy/depth regions in Figure 2.4. The color table at the bottom of the figure records how many states (of 35 observed) fall into each differential region of energy-depth space identified by a color.

identified by different colors. For example, state 1 in Figure 2.2c has an average depth of 0.13nm and average energy of 3.5 eV above the dielectric valence band, and state 2 has an average depth of 0.15nm and an average energy of either 3.2 eV or 3.8 eV. The energy ambiguity for state 2 is reflected in Figure 2.4 by the fact that regions of the same color are found both above and below 3.5 eV (right axis). This ambiguity comes from the fact that an AC voltage is used to shuttle the electron, and only the magnitude of the trap state energy relative to the tip Fermi level at flat band can be determined. In the future, this ambiguity will be eliminated by performing single electron tunneling force spectroscopy (frequency shift versus voltage curves) [30] over each observed state in the DTFM images. The finite resolution of the energy and depth determination is due to the finite intervals of z_{min} and V_{ac} chosen in experiment. The uncertainty in tip/surface gap determination of ~(±0.15nm) leads to a depth uncertainty of ±0.2nm and an energy uncertainty of ±(0.1eV) in the energy-depth measurements.

Using the data obtained with the maximum V_{ac} applied voltage (+/- 3V) and minimum gap z_{min} (0.5 nm) to image this sample, the average density of states between ~2.5 eV and ~4.5 eV above the dielectric valence mobility edge and within ~ 0.8 nm depth of the surface is determined to be 1×10^{19} cm^{-3} eV^{-1}. This direct measurement of the density of states is unique in that it does not depend on the state's initial charge occupation or spin. The method also provides a direct determination of the real space distribution of states.

It is noteworthy that in this particular film, the density of states is not uniformly distributed with respect to energy or depth. For example, in Figure 2.4 there are 8 of 35 total states that are concentrated in the adjoining green and yellow areas, and another 8

states located in the adjoining blue and red areas, but no states in any of the black regions. This quantitative measure of the density of trap states is not easily determined by other methods. Further improvements to the methodology will provide a unique quantitative determination of the energy and depth of every individual state accessible to tunneling.

In summary, Dynamic Tunneling Force Microscopy measurements are performed on an interlayer dielectric film with height and surface potential feedback control, providing images of trap state distribution, surface potential and topography. The images indicate that little correlation exists between the trap state locations and the local surface potential or topography of the film. The energy and depth of the trap states is calculated using a tunneling model. The average density of states is quantitatively determined to be $1\times10^{19}cm^{-3}eV^{-1}$ near the dielectric surface and in the energy range from 2.5 to 4.5 eV above the valence edge. This direct measurement of the spatial distribution and average density of trap states will be useful in understanding dielectric materials needed for future device applications.

The authors would like to thank the Semiconductor Research Corporation for funding this work.

2.3 References

[1] *Solid-State Physics: An Introduction to Principles of Materials Science*, edited by H. Ibach and H. Luth (Springer, 4th edition, 2009), Chap.11

[2] K. Maex, M. R. Baklanov, Denis Shamiryan, S. H. Brongersma, and Z. S. Yanovitskaya, J. Appl. Phys. 93, 8793 (2003).

[3] K. Y. Yiang, W. J. Yoo, Q. Guo, and A. Krishnamoorthy, Appl. Phys. Lett. 83, 524 (2003).

[4] J. M. Atkin, T. M. Shaw, E. Liniger, R. B. Laibowitz, and T. F. Heinz, Reliability Physics Symposium (IRPS), 2012 IEEE International, pp. BD-1. IEEE, 2012.

[5] G. G. Gischia, K. Croes, G. Groeseneken, Z. Tokei, V. Afanas' ev, and L. Zhao, Reliability Physics Symposium (IRPS), 2010 IEEE International, pp. 549-555. IEEE, 2010.

[6] B. C. Bittel, P. M. Lenahan, and S. W. King, Appl. Phys. Lett. 97, 063506 (2010).

[7] H. Ren, M. T. Nichols, G. Jiang, G. A. Antonelli, Y. Nishi, and J. L. Shohet, Appl. Phys. Lett. 98, 102903 (2011).

[8] C. J. Cochrane and P. M. Lenahan, Appl. Phys. Lett. 104, 093503 (2014).

[9] J. M. Atkin, E. Cartier, T. M. Shaw, R. B. Laibowitz, and T. F. Heinz, Appl. Phys. Lett. 93, 122902 (2008).

[10] J. M. Atkin, D. Song, T. M. Shaw, E. Cartier, R. B. Laibowitz, and T. F. Heinz, J. Appl. Phys. 103, 094104 (2008).

[11] H. Sinha, H. Ren, M. T. Nichols, J. L. Lauer, M. Tomoyasu, N. M. Russell, G. Jiang, G. A. Antonelli, N. C. Fuller, S. U. Engelmann, Q. Lin, V. Ryan, Y. Nishi, and J. L. Shohet, J. Appl. Phys. 112, 111101 (2012).

[12] S. King, H. Simka, D. Herr, H. Akinaga, and M. Garner, APL Mater. 1, 40701 (2013).

[13] M. E. Welland and R. H. Koch, Appl. Phys. Lett. 48, 724 (1986).

[14] T. Ruskell, R. Workman, D. Chen, D. Sarid, S. Dahl, and S. Gilbert, Appl. Phys. Lett. 68, 93 (1996).

[15] B. Kaczer, Z. Meng, and J. P. Plez, Phys. Rev. Lett. 77, 91 (1996).

[16] R. Ludeke and E. Cartier, Appl. Phys. Lett. 78, 3998 (2001).

[17] L. J. Klein and C. C. Williams, Appl. Phys. Lett. 81, 4589 (2002).

[18] Y. Naitou, H. Arimura, N. Kitano, S. Horie, T. Minami, M. Kosuda, H. Ogiso, T. Hosoi, T. Shimura, and H. Watanabe, Appl. Phys. Lett. 92, 012112 (2008).

[19] J. P. Johnson, N. Zheng, and C. C. Williams, Nanotechnology 20, 055701 (2009).

[20] E. Bussmann, D. J. Kim, and C. C. Williams, Appl. Phys. Lett. 85, 2538 (2004).

[21] E. Bussmann, N. Zheng, and C. C. Williams, Appl. Phys. Lett. 86, 163109 (2005)

[22] W. Melitz, J. Shen, A. C. Kummel, and S. Lee, Surf. Sci. Rep. 66, 1 (2011).

[23] S. King, B. French, and E. Mays, J. Appl. Phys. 113, 44109 (2013).

[24] R. Wang, and C. C. Williams, unpublished.

[25] J. P. Johnson, D. W. Winslow, and C. C. Williams, Appl. Phys. Lett. 98, 052902 (2011).

[26] N. Zheng, C. C. Williams, E. G. Mishchenko, and E. Bussmann, J. Appl. Phys. 101, 093702 (2007).

[27] J. Borja, J. L. Plawsky, T. M. Lu, H. Bakhru and W. N. Gill, J. Appl. Phys. 115 , 084107 (2014).

[28] Chanhyung Kim, Journal of the Korean Physical Society, Vol. 47, November 2005, pp417.

[29] H. Zheng, S. W. King, V. Ryan, Y. Nishi and J. L. Shohet, Appl. Phys. Lett. 104, 062904 (2014).

[30] E. Bussmann, and C. C. Williams, Appl. Phys. Lett. 88, 263108 (2006).

CHAPTER 3

THEORETICAL DERIVATION OF DYNAMIC TUNNELING FORCE MICROSCOPY SIGNAL AMPLITUDE AND COMPARISON BETWEEN SIMULATION AND EXPERIMENTAL RESULTS

This chapter contains a paper that was submitted for publication in Review of Scientific Instrument entitled Dynamic Tunneling Force Microscopy for characterizing electron trap states in nonconductive surfaces by R. Wang and C. C. Williams.

Dynamic tunneling force microscopy is a scanning probe technique for real space mapping and characterization of individual electronic trap states in nonconductive films with atomic scale spatial resolution. In this chapter, the physical basis for the DTFM method is unfolded through a theoretical derivation of the dynamic tunneling signal amplitude as a function of several experimental parameters. Experimental data are compared with the theoretical simulations, showing quantitative consistency and verifying the physical model used. The experimental system is described and representative imaging results are shown.

3.1 Introduction

Dynamic Tunneling Force Microscopy (DTFM) is a technique which is used to image and characterize atomic scale electronic trap states in nonconductive films and

surfaces [1]. DTFM provides a 2D map of these states and can provide a direct measure of the energy and depth of each individual trap state [2,3]. While methods already exist which measure the averaged properties of an ensemble of defect states in a dielectric or semiconducting film, such as electron paramagnetic resonance (EPR) [4], electrically detected magnetic resonance (EDMR) [5], and conductance and capacitance techniques [6], DTFM enables characterization of each state individually in real space. Scanning probe microscopy methods such as scanning tunneling microscopy (STM) [7], conductive atomic force microscopy (c-AFM) [8], ballistic electron emission microscopy (BEEM) [9], Kelvin probe force microscopy (KPFM) and electrostatic force microscopy (EFM) [10,11], and scanning capacitance microscopy (SCM) [12] have also been employed to characterize local electronic properties of dielectric films. However, STM, c-AFM and BEEM are limited by the requirement that a detectable current must be measured and therefore can be applied only to films with adequate conductance. KPFM and EFM only measure charge in trap states. These methods are therefore not sensitive to trap states which are neutral. Atomic scale SCM imaging has not been achieved due to either finite probe tip radius or limited sensitivity. When compared to these methods, DTFM can image trap states, whether charged or uncharged, with atomic scale spatial resolution [1] and can be applied to completely nonconducting surfaces. This work presents the theoretical basis of the DTFM method and a detailed description of the methodology.

Dynamic Tunneling Force Microscopy is based upon concepts of single electron tunneling originally demonstrated through quasi-static Atomic Force Microscopy (AFM) measurements. Single electron tunneling between a metallic AFM tip and a trap state in a

dielectric surface was first observed by Klein using an AFM amplitude modulation mode [13] and by Bussmann using an AFM frequency modulation mode [14,15]. Quantitative analysis was performed verifying that single electron tunneling events were being detected [14]. Dana [16] and Stomp [17] also detected single electron tunneling by AFM, but the tunneling in these studies takes place between the trap states and substrate rather than between probe tip and trap states. In Dynamic Tunneling Force Microscopy, the signal comes from the dynamic tunneling (shuttling) of single electrons between a metallic AFM probe tip and individual trap states in the dielectric surface under an applied bipolar voltage (shuttling voltage). The shuttled electron produces a periodic electrostatic force on the AFM probe tip which is detected at the frequency of the shuttling voltage. Because the electron shuttles many times between tip and a given trap state, the DTFM signal does not depend upon the initial occupancy of the trap state, i.e. it can have an initially positive, neutral, or negative charge.

A derivation of the static electrostatic force acting on a metallic probe tip near a dielectric surface with and without a charge in a nearby trap state is shown in the following section. The analysis is then extended to the dynamic electron shuttling case.

3.2 Electrostatic Force Induced Frequency Shift

Consider the configuration of a metallic AFM tip above a dielectric surface with an electronic trap state at a particular depth in the dielectric film. A simple one-dimensional parallel plate capacitor model is used to calculate the electrostatic force sensed by the AFM tip. The parallel plate capacitor contains three regions as shown in Figure 3.1, including the region between the tip and the dielectric surface, the dielectric surface and the trap state, and the trap state and the sample back-contact. Bussmann [18]

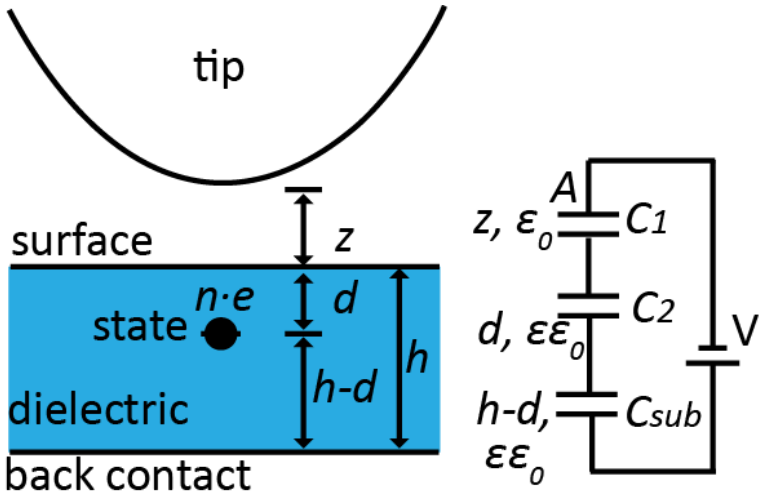

Figure 3.1 Configuration of a metal tip above an electron trap state in a dielectric film, and the corresponding one-dimensional parallel plate capacitor model. z is the tip-surface gap, d is the depth of trap state in dielectric film, h is the thickness of dielectric film. C_1 , C_2, and C_{sub} are the capacitances between the tip and the dielectric surface, the surface and the trap state, the trap state, and the sample back-contact, respectively, and V is the voltage applied between the tip and sample back-contact.

compared the results of this one-dimensional parallel plate model to results from more sophisticated three-dimensional electrostatic tip-surface models which take into account the localization of the charge and spherical tip profile. It was found that the simple one-dimensional model is good approximation to the more complex models. The one-dimensional parallel plate model is used in this paper because it provides an analytical expression for the DTFM signal amplitude, showing the explicit dependency on experimental parameters.

The free energy of the system for the one-dimensional model shown in Figure 3.1 can be written as [19]

$$E = \frac{(ne)^2}{2\left(C_{sub} + C_{tip}\right)} - \frac{C_{sub}}{C_{sub} + C_{tip}} neV - \frac{1}{2}\frac{C_{sub}C_{tip}}{C_{sub} + C_{tip}} V^2 \ , \tag{3.1}$$

where n is the number of electrons in the trap state, e is charge of the electron, and V is the voltage applied between the tip and sample back-contact. $C_{tip} = C_1C_2/(\,C_1 + C_2)$ where $C_1 = \varepsilon_0 A/z$, $C_2 = \varepsilon\varepsilon_0 A/d$, and $C_{sub} = \varepsilon\varepsilon_0 A/(h-d)$. The tip area is A, tip-surface gap is z, the state depth is d, the film thickness is h, permittivity of vacuum is ε_0, and the sample dielectric constant is ε. The static force acting on the tip F can be obtained by $F = -\partial E/\partial z,$ yielding

$$F = \frac{1}{2}\frac{\partial C_{series}}{\partial z}\left(V - \frac{ne}{C_{sub}}\right)^2, \tag{3.2}$$

where $C_{series} = (\,C_{tip}C_{sub}\,)/(C_{tip} + C_{sub})$. The resonance frequency shift (df) of an oscillating AFM cantilever when it is close to the surface is related to the force acting on the probe tip $F(z)$ through relationship [20],

$$df = \frac{f_0^2}{ka}\int_0^{1/f_0} F(z)cos(2\pi f_0 t)dt, \tag{3.3}$$

where f_0 is resonance frequency of the cantilever, k is the spring constant, a is oscillation amplitude of the AFM cantilever, and t is time. Time dependence of the tip height is $z = z_0 + a(1 + cos(2\pi f_0 t))$, where z_0 is the minimum tip-sample gap. If we insert (3.2) into (3.3) and integrate, the frequency shift becomes [18]

$$df = -\frac{f_0}{2k}\frac{\varepsilon_0 A\left(V - \frac{ne}{C_{sub}}\right)^2}{\left(z_0 + \frac{h}{\varepsilon}\right)^{\frac{3}{2}}\left(z_0 + 2a + \frac{h}{\varepsilon}\right)^{\frac{3}{2}}}. \tag{3.4}$$

This equation quantitatively describes the frequency shift of the oscillating AFM probe tip as a function of the number of electrons (n) in the trap state. It also includes the explicit dependence of the frequency shift on all other relevant experimental parameters, such as the characteristics of the AFM cantilever (f_0, k), cantilever oscillation amplitude (a), probe tip area (A), dielectric film properties (h, ε), depth of trap state (d, which is included in C_{sub}), minimum tip-sample gap (z_0), and applied voltage (V). Note that equation (4) is a general form of df corresponding to the electrostatic model shown in Figure 3.1. In the DTFM method, V, z_0, and n in equation (3.4) take on specific time dependent forms as detailed below.

3.3 Dynamic Tunneling Force Microscopy Signal

Elastic tunneling between a trap state and a metallic tip is governed by two conditions. The first is that the electron trap state must be close enough to the metallic tip that the probability for tunneling is adequately high so that tunneling events are likely to

occur. The tunneling rate is determined by the tunneling barrier height and width. Thus the tip-sample gap, tip work function, physical depth, and energy of the trap state in the band gap of the dielectric material all determine which states can be accessed by tunneling. Calculations of the tunneling rate as a function of the trap state energy and depth, tip-sample gap, and tip work function have been performed by Zheng [21]. The second condition is determined by the occupancy of the states involved in the tunneling. Electrons in *filled* states in the probe tip can elastically tunnel into *empty* trap states at the same energy in the surface or visa versa. Since the probe tip is metallic, the Fermi-level of the tip determines the occupancy of states in the tip. States above tip Fermi level are empty and below are filled. Bussmann demonstrated that a single electron can be induced to tunnel back and forth between the tip and a trap state in the surface at two distinct static applied voltages [22]. In a similar way, a periodic bipolar voltage is applied in DTFM to induce dynamic electron shuttling between tip and trap states in surface.

In the DTFM method [1], an AC voltage is used to periodically move the Fermi-level of the probe tip up and down with respect to energy levels in the dielectric film. Assuming an empty trap state exists in the dielectric surface within tunneling range of the tip, when the tip Fermi level moves above the energy of that trap state, an electron in the metal tip which is aligned energetically with the trap state will elastically tunnel from the tip to the trap state. When the applied voltage changes to the other polarity, the tip Fermi level moves below the energy of the trap state in the sample surface, and the electron in that particular trap state will tunnel back into the probe tip. In this way, the AC voltage causes a periodic single electron shuttling between the tip and the trap state. This electron shuttling produces the DTFM signal.

In more detail, a shuttling voltage (temporally asymmetric square wave voltage) V_{ac} is applied between the sample back-contact and probe tip to induce electron shuttling. Simultaneously, the minimum tip-sample gap is sinusoidally modulated by a few nanometers, which brings the tip in and out of tunneling range at exactly twice the frequency of the applied shuttling voltage. The applied voltage (V_{ac}) and height modulation (z_{mod}) are synchronized, as shown in Figure 3.2. Because of the exponential dependence of the tunneling rate on tip-sample gap (typical tunneling rate changes by an order of magnitude per Angstrom), the electron tunneling to a trap state occurs only when the tip is near its minimum tip-sample gap (z_{min}). This timing causes the trap state occupancy $n_0(t)$ waveform to be shifted by 90 degrees in phase relative to the applied voltage V_{ac}. This can be observed in Figure 3.2 by comparing the relative position of the applied shuttling voltage waveform $V_{ac}(t)$ with that of the trap state occupancy waveform $n_0(t)$. Each time the probe tip reaches this minimum height, the polarity of the applied shuttling voltage has been reversed, when compared to the previous minimum, causing the electron to alternatively tunnel to and from the trap state in the surface.

This phase shift provides a way to separate out the component of the frequency shift df signal due to dynamic electron shuttling (DTFM signal) which is out of phase with V_{ac}, from a df signal component which is in-phase with the applied shuttling voltage (V_{ac}) using a two phase lock-in amplifier. The following quantitatively analysis shows that the 90 degree phase shifted component (DTFM signal) is proportional to the number of shuttling electrons and therefore it is the signal needed to detect trap states. The in-phase signal is proportional to the difference between the tip and local surface potential. This signal is kept at zero by adjusting the applied DC voltage V_{DC} using a feedback loop.

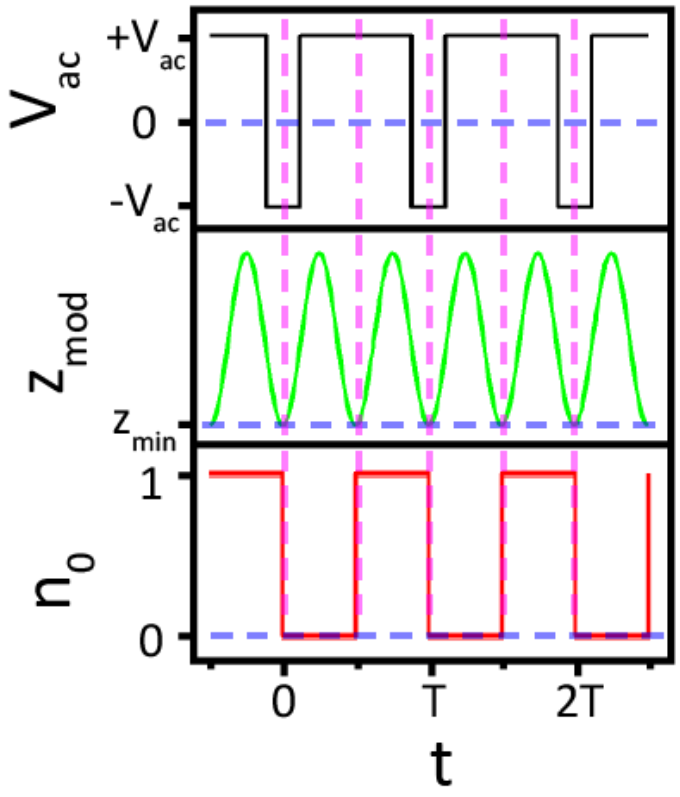

Figure 3.2 Time dependencies of shuttling voltage V_{ac}, tip height modulation z_{mod}, and trap state occupation n_0 in DTFM design. T is the period of V_{ac}, with $T = 1/f_{sh}$.

This compensating voltage provides a map of the local surface potential, as in standard Kelvin Probe Force Microscopy (KPFM) [23]. Thus, the method described here detects and images electronic trap states through electron shuttling, and simultaneously provides height and surface potential (KPFM) images.

Figure 3.2 shows the temporally asymmetric square wave shuttling voltage V_{ac} applied between the sample back-contact and probe tip, with a typical frequency of ~300 Hz. A tip height modulation (z_{mod}) of approximately 2 nm at a frequency exactly twice that of V_{ac} (~600 Hz) is also introduced. This height modulation is independent of the tip oscillation of the cantilever at its resonance frequency ~270kHz, which typically has an oscillation amplitude of 10 nm. The corresponding electron occupancy in the surface state $n_0(t)$ is also shown, with the appropriate phase relation to V_{ac}. Under these conditions, the frequency shift df signal, as shown by equation (3.4), is detected by a FM detector and the output is sent to a two-phase lock-in amplifier, as is shown in Figure 3.3 and discussed below. The lock-in amplifier detects both the in-phase (surface potential) signal and the 90 degree phase (DTFM) signal independently.

To quantitatively derive the DTFM signal, the terms V (applied voltage), z_0 (tip height), and n(number of electrons in the trap state) found in equation (4.4) are replaced with the corresponding time-dependent terms $V(t) = (V_{DC} - V_{SP}) + V_{ac}(t)$, $z_0 = z_{mod}(t)$, and $n(t) = N \cdot n_0(t)$. The waveforms and synchronization of $V_{ac}(t)$, $z_{mod}(t)$, and $n_0(t)$ are shown in Figure 3.2. V_{DC} is the applied DC voltage, V_{SP} is the local surface potential of the sample below the probe tip, and N is the number of electrons being shuttled, providing for a way to account for the case in which more than one state exists under the tip. The minimum tip-sample gap during tip height modulation $z_{mod}(t)$,

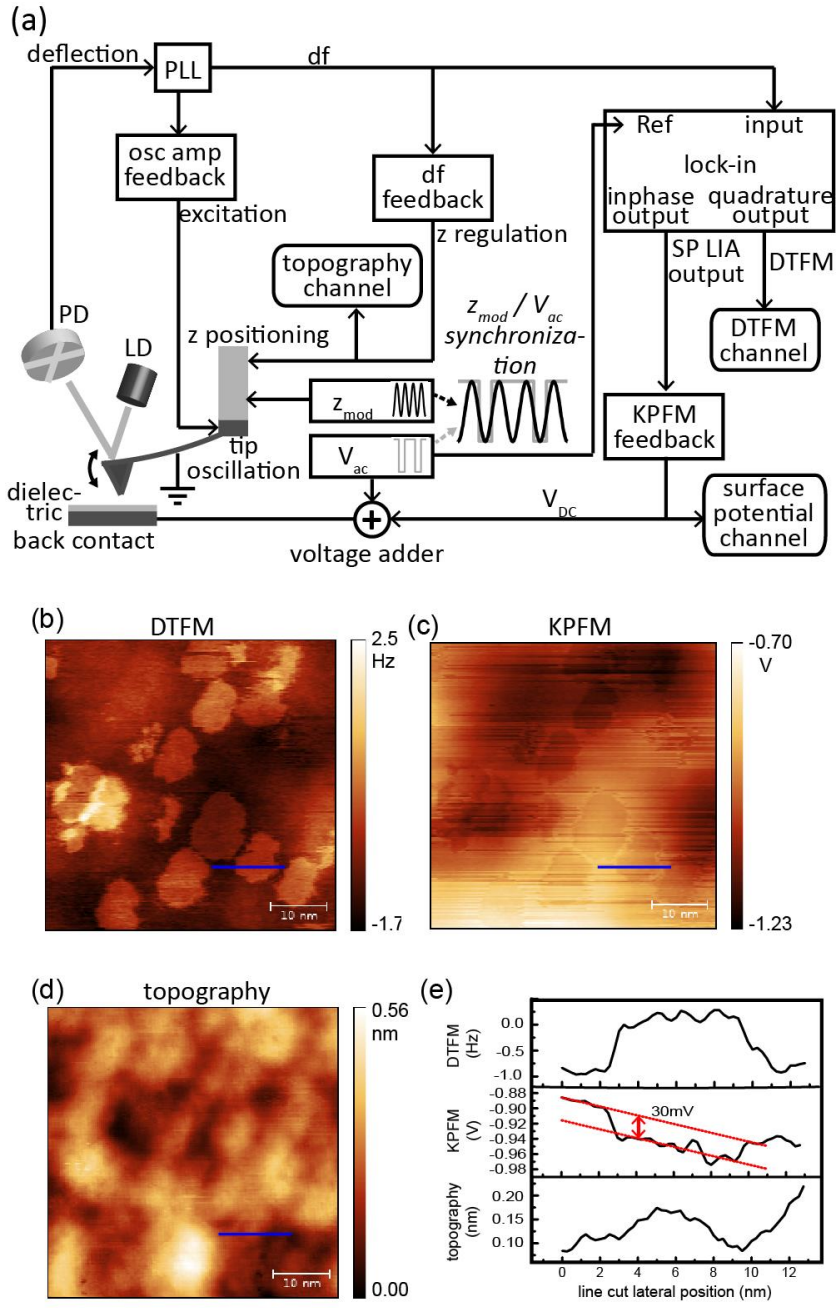

Figure 3.3 DTFM experimental set-up and image data. (a) DTFM experimental set-up. The photodiode, laser diode, phase lock loop, and tip oscillation amplitude feedback loop are denoted as PD, LD, PLL, and osc amp feedback. (b), (c) and (d) are DTFM, surface potential (KPFM), and topography images taken simultaneously on a 6nm low-k ILD film (k=3.3) a-$SiO_{1.2}C_{0.35}$:H fabricated at Intel Corporation [24]. Line cuts at the same locations of images in (b),(c), and (d) at the blue lines are shown in (e). ((a)-(d) are reprinted with permission from Reference [2].)

is denoted as z_{min}, as shown in Figure 3.2.

After these time-dependent terms are substituted into equation (3.4), it can be shown that the only term contributing to df at frequency f_{sh} (Fourier component) is the $\left(V - \frac{ne}{C_{sub}}\right)^2$ term, because the only other term which is time-dependent in equation (3.4) is the $z_{mod}(t)$ term, which varies at a frequency of $2f_{sh}$. If the $\left(V - \frac{ne}{C_{sub}}\right)^2$ term is expanded to include the time-dependent terms, the parts which produce the in-phase and quadrature components with respect to V_{ac} can be seen.

$$\left(V - \frac{ne}{C_{sub}}\right)^2 = ((V_{DC} - V_{SP}) + V_{ac}(t) - \frac{Ne}{C_{sub}} n_0(t))^2$$

$$= (V_{DC} - V_{SP})^2 + V_{ac}(t)^2 + 2(V_{DC} - V_{SP})V_{ac}(t) + \left(\frac{Ne}{C_{sub}}\right)^2 n_0(t)$$

$$-2(V_{DC} - V_{SP})\frac{Ne}{C_{sub}} n_0(t) - 2\frac{Ne}{C_{sub}} V_{ac}(t)\, n_0(t)\,. \qquad (3.5)$$

Note that the $(V_{DC} - V_{SP})^2$ term is constant in time. The $V_{ac}(t)^2$ term is also constant with time, because $V_{ac}(t)$ has positive and negative values with equal magnitudes. The $2(V_{DC} - V_{SP})V_{ac}(t)$ term is in-phase with $V_{ac}(t)$. The $\left(\frac{Ne}{C_{sub}}\right)^2 n_0(t)$ and $-2(V_{DC} - V_{SP})\frac{Ne}{C_{sub}} n_0(t)$ terms are 90 degree phase shifted with respect to $V_{ac}(t)$, because $n_0(t)$ is 90° phase shifted with respect to $V_{ac}(t)$. The term $-2\frac{Ne}{C_{sub}} V_{ac}(t)\, n_0(t)$ contributes to both in-phase and quadrature components.

There are only two terms that can contribute to the *in-phase* df signal component , $2(V_{DC} - V_{SP})V_{ac}(t)$ and $-2\frac{Ne}{C_{sub}} V_{ac}(t)\, n_0(t)$. In the DTFM method, the *df* in-phase component is detected by a lock-in amplifier referenced at 0 degrees (in-phase) relative to

V_{ac}(t). A feedback loop, shown in Figure 3.3(a), is employed to keep this in-phase component at zero, by adjusting the applied DC voltage (V_{DC}). The DC voltage thus follows the local surface potential, as in KPFM [23]. Under these conditions, it can be shown that the applied voltage V_{DC} is given by

$$V_{DC} = V_{SP} + \frac{\frac{1}{2}Ne}{C_{sub}} = V_{SP} + \frac{1}{2}\frac{(h-d)Ne}{\varepsilon\varepsilon_0 A}. \quad (3.6)$$

Thus, with a feedback loop maintaining the in-phase component at zero, when no electron shuttling occurs (N=0), $V_{DC} = V_{SP}$, as in the conventional KPFM method, i.e. the applied DC voltage V_{DC} is equal to the local surface potential V_{SP}. When an electron is being shuttled (N ≠ 0), V_{DC} compensates for both the local surface potential (V_{SP}) and an additional term ($\frac{1}{2}\frac{(h-d)Ne}{\varepsilon\varepsilon_0 A}$) which corresponds to the additional average surface potential caused by the shuttled charge (Ne). The factor ½ is there because when charge is shuttled, it spends only half of the time in the trap state and the other half in the tip (see Figure 3.2). This extra surface potential is typically small (~30 mV), but can be observed in surface potential images when an electron is shuttling. Experimental data are shown in the experimental section below.

The terms which contribute to the quadrature component of the df signal with respect to V_{ac}(t) are $\left(\frac{Ne}{C_{sub}}\right)^2 n_0(t) - 2(V_{DC} - V_{SP})\frac{Ne}{C_{sub}} n_0(t) - 2\frac{Ne}{C_{sub}} V_{ac}(t)\, n_0(t)$. While under KPFM feedback control, the first two terms of the three quadrature component terms above cancel with each other, using equation (3.6), and only the third term is left. After substitution of this remaining quadrature term of $\left(V - \frac{ne}{C_{sub}}\right)^2$ into

equation (3.4) a Fourier transform is performed (equation (3.7)) to obtain the quadrature component of df, which is the DTFM signal. Because the DTFM signal is a component of df, it has unit of Hz.

$$DTFM\ signal = \frac{\sqrt{2}f_0 eN(h-d)}{k\varepsilon T}\int_0^T \frac{V_{ac}(t)\, n_0(t)}{\left(z_0(t)+\frac{h}{\varepsilon}\right)^{\frac{3}{2}}\left(z_0(t)+2a+\frac{h}{\varepsilon}\right)^{\frac{3}{2}}}\cos(2\pi f_{sh}t + 90°)\, dt. \quad (3.7)$$

This equation provides the theoretical basis for the DTFM operation. First, it shows that the DTFM signal is proportional to the number of shuttling electrons (N). As the probe tip is scanned over a trap state, electron shuttling occurs and the DTFM signal rises, producing a 2D image of the trap states in the dielectric surface. Secondly, based on this model, the DTFM amplitude does not depend on tip area (A). This is important because the tip area is difficult to define and characterize in a real experiment. The tip area independence makes it possible for quantitative comparison between theoretical and experimental results of DTFM signal amplitudes without explicit knowledge of the exact tip profile. Thirdly, the DTFM amplitude is proportional to the distance between the state and the back-contact ($h-d$). This indicates that the DTFM signal is small when the trap state is deep in the surface and maximum when the state is near the surface. Fourthly, the DTFM signal amplitude is proportional to the applied shuttling voltage amplitude V_{ac}. And finally, the DTFM signal decreases as the tip-sample gap increases.

3.4 Experimental Description

DTFM measurements are performed with an Omicron Multiprobe S atomic force microscope under a vacuum of 10^{-10} mBar at room temperature. A metal coated AFM probe (Nanosensors PPP-NCHPt), with ~10 nm tip oscillation amplitude at its nominal resonance frequency f_0 ~ 270 kHz and stiffness ~40 N/m, is brought within tunneling range of a dielectric surface. A periodic temporally asymmetric square wave shuttling voltage (V_{ac}) at ~300 Hz frequency (f_{sh}) is applied to the sample back-contact with tip grounded, consisting of a positive voltage ($+V_{ac}$) for 77% of its duty cycle and a negative voltage ($-V_{ac}$) for the remaining 23%. The probe height modulation (z_{mod}) is at $2f_{sh}$ frequency (~ 600 Hz) and has an amplitude of 2nm, which is independent of the tip oscillation at ~ 270 kHz (probe resonance frequency). The voltage and height modulations are synchronized as in Figure 3.2. The cantilever frequency shift (df) signal is measured by a PLL detector and goes to a two phase lock-in amplifier, referenced by V_{ac}, as shown in Figure 3.3(a). The lock-in amplifier separately detects the in-phase and quadrature components of the df signal. The in-phase component is proportional to the difference between the tip and local surface potential. The KPFM feedback loop adjusts the applied voltage (V_{DC}) to keep the in-phase df component at zero. With the KPFM feedback loop on, this applied voltage (V_{DC}) is a measure of the local surface potential, as in standard KPFM [23]. The quadrature component of the frequency shift df is the DTFM signal.

During imaging, the z piezo voltage is adjusted to follow the surface topography variation using a height control feedback loop, which keeps the average frequency shift df constant. This keeps the tip-sample gap z_{min} at an approximately constant value during

imaging. Since df is modulated by the applied voltage V_{ac} (~300 Hz) and height modulation z_{mod} (~600Hz), the gain of the height feedback control loop is adjusted to respond slowly (below 300 Hz), so that it follows only the averaged (filtered) df signal. To acquire DTFM images, the tip is pulled back by a chosen distance from the position at which the df-z curve reaches a minimum value. This distance is used as an estimated tip-surface gap z_{min}. This estimate is discussed in the following section. Three separate images are acquired during DTFM imaging by recording the DTFM signal (DTFM image), the applied compensating voltage V_{DC} under KPFM feedback control (KPFM image) and the z piezo movement as adjusted by the height control feedback loop (topography image).

Figure 3.3 shows DTFM (b), KPFM (c), and topography (d) images acquired simultaneously on a 6nm low-k ILD film (k=3.3) a-$SiO_{1.2}C_{0.35}$:H. Each bright spot in the DTFM image represents a trap state. The apparent size of the states in the DTFM image is due to a tip imaging effect [1,2]. The trap states typically have physical dimensions on the order of a few Angstroms [25]. When the AFM probe tip is scanned over the state, tunneling can occur over a finite lateral region of the tip apex, producing an apparent state size which is much larger than the state itself. The apparent shape of the states in the image reveals the shape of the AFM tip apex. States at larger depths appear smaller in the images. A slow varying background is also present in the DTFM image. This background is still under study, but is most likely due to imperfect phasing of the lock-in amplifier. Trap state images on several different dielectric surfaces have been performed [1, 2].

Comparison of the DTFM, surface potential, and topography images shows little

correlation between the trap state locations and the KPFM and topography images. Note that the corrugation of the surface is small (< 0.6 nm). However, there is a small amount of coupling between the KPFM and DTFM images, that is, surface potential (KPFM) shows small changes at the locations where electron shuttling to trap states is occurring. Line cuts across a trap state at the same location in the DTFM, KPFM, and topography images are shown in Figure 3.3(e). When electron shuttling occurs, the KPFM signal shows an offset of ~30mV compared to surrounding regions after subtracting a linear background. This is consistent with the theoretical analysis presented above (equation (3.6)), which predicts the shuttling electron will cause a change in surface potential corresponding to half of its charge.

Figure 3.4 shows a series of DTFM images acquired on the same area of a dielectric film ($SiO_{0.55}C_{0.7}$:H) [26] with different AC voltage amplitudes and tip heights. Figure 3.4 (a) and (b) have the same z_{min} but different V_{ac}. With a larger AC voltage amplitude, DTFM detects trap states within a larger energy range due to the larger movement of the tip Fermi level; therefore, more states are accessed as in Figure 3.4 (b) compared to 3.4 (a). Figure 3.4 (c) and (d) have the same V_{ac} but different z_{min}. Decreasing the tip-surface distance allows for tunneling to states deeper in the dielectric film, which explains why more states are detected in Figure 3.4 (d) than in Figure 3.4 (c). Energy and depth of individual states can be extracted using the values of the applied shuttling voltage (V_{ac}) and the probe height (z_{min}) at which a state appears, as demonstrated in Reference [2].

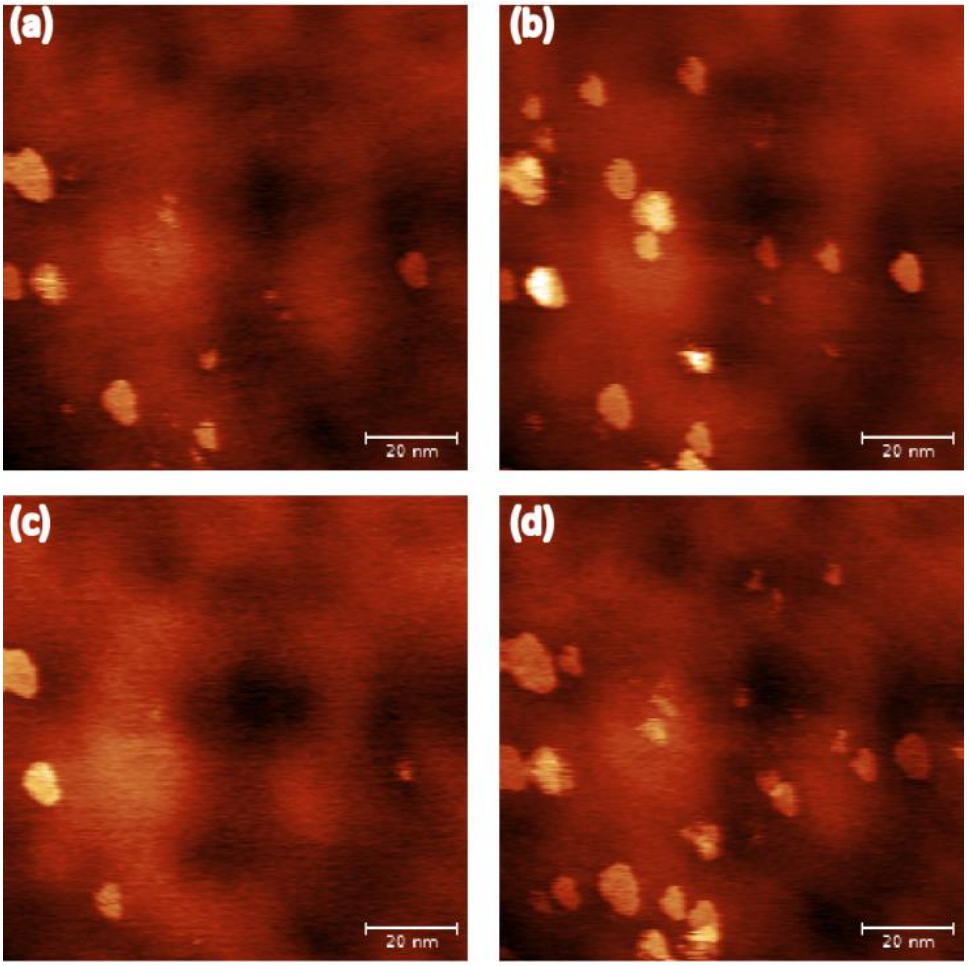

Figure 3.4 Comparison of DTFM images acquired in the same area of a dielectric surface at different applied AC voltages and probe heights. (a) V_{ac}=2V, z_{min}=1.1nm; (b) V_{ac}=4V, z_{min}=1.1nm; (c) V_{ac}=2V, z_{min}=1.3nm; (d) V_{ac}=2V, z_{min}=0.9nm.

3.5 Comparison of Theoretical Predictions with Measurement

To verify the DTFM theory, the dependencies of DTFM signal amplitude on shuttling electron number, AC voltage amplitude, and tip-surface gap are quantitatively compared with experimental results.

A histogram of DTFM amplitudes for all states in the DTFM image shown in Figure 3.5(a) is presented in Figure 3.5(b). The mean value and standard deviation of the DTFM amplitude of a given state are measured by performing six line cuts across aparticular state in different directions and subtracting their linear backgrounds. This is done to reduce the effect of the varying background in DTFM image. The histogram shows a dominant peak, which has a mean value of 0.86Hz and standard deviation of 0.21 Hz, determined by a Gaussian fit, and one separate data point at 1.72 Hz. The DTFM amplitude for single electron shuttling in this specific experiment can be calculated using equation (3.7). The blue dashed lines are the calculated DTFM using parameters from this experiment, which include the resonance frequency of the cantilever (259kHz), cantilever stiffness (30N/m), oscillation amplitude (10nm), dielectric thickness (6nm), dielectric constant (3.3), V_{ac} (2V), and z_{min} (0.5nm).

The depths of the trap states (d) likely vary and are not known, but a previous tunneling calculation [2] predicts tunneling is unlikely to reach states deeper than ~ 1 nm in this experiment. The calculated values of the DTFM amplitude, assuming one electron shuttling, for a state depth of 0nm (on surface) is 1.04 Hz and for 1nm depth is 0.87 Hz. The absolute value of the DTFM amplitudes from simulation and experiment show a good consistency. It is worthy of note that the experimental DTFM amplitudes are

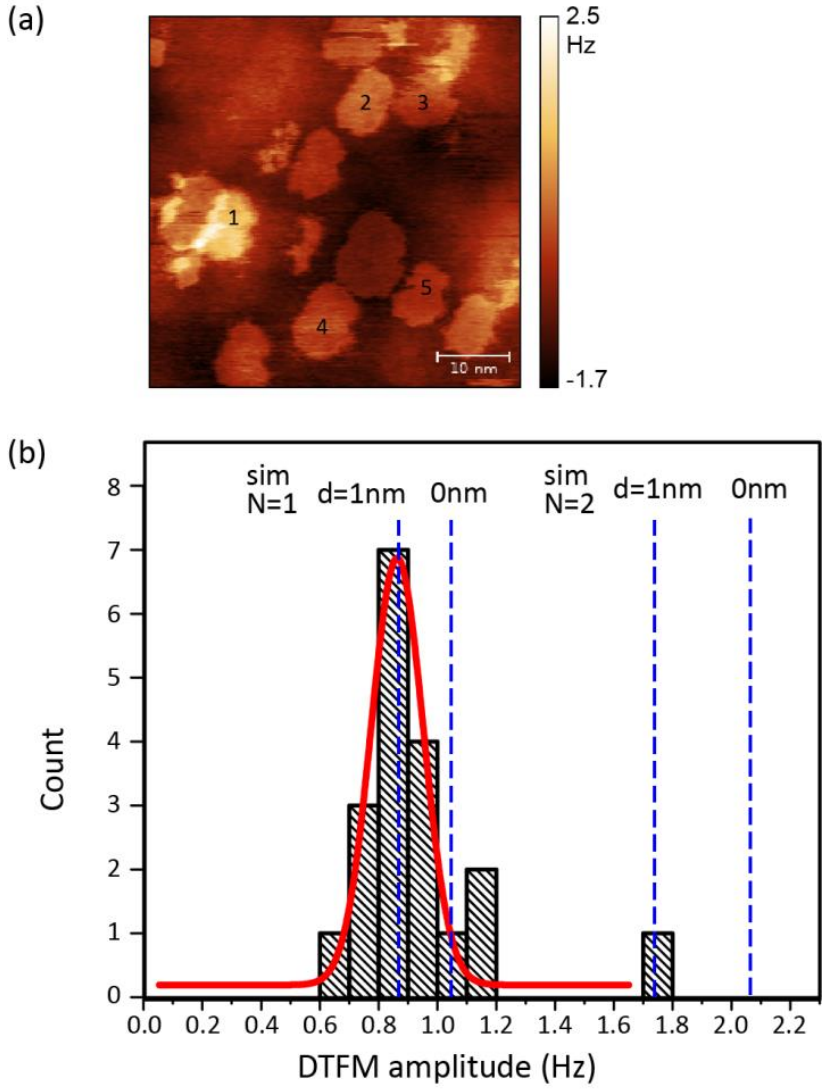

Figure 3.5 Histogram of DTFM signal amplitudes in a DTFM image. (a) A DTFM image (V_{ac}=2V, z_{min}=0.5nm) on a 6nm a-$SiO_{1.2}C_{0.35}$:H film. Five states are marked in the image for reference. (b) Histogram of DTFM amplitudes of all trap states observed in (a). The red curve is a Gaussian fit to the data below 1.7Hz, with mean value 0.86Hz and standard deviation 0.21 Hz. The blue dashed lines show simulated DTFM amplitudes for shuttling electron number N=1 and N=2 at trap state depths d=0 nm and d=1 nm.

distributed over a larger range than expected from variation of state depths. This spread in DTFM amplitude is likely due to uncertainties encountered in extraction of the DTFM amplitudes. The standard deviations of the DTFM amplitude measured from 6 line cuts on each state have an average value of 0.13Hz. This relatively large standard deviation comes from the difficulty in dealing with the presence of the irregular background in DTFM images. The separate data point at 1.72Hz is measured in a location labeled state 1 in Figure 3.5(a). The DTFM amplitude at this location is about twice the value of DTFM amplitude peak for single electron shuttling, and is also consistent with a simulated value for two electron shuttling. It is likely due to tunneling to two states that are very close together.

The linear dependency of the DTFM signal amplitude on V_{ac} is displayed in Figure 3.6(a), with a general consistency shown between the experimental data (four states) and the simulation results. The DTFM signal versus z_{min} is also examined in Figure 3.6 (b). Again, a general agreement is observed between experimental and simulation results. The slow change of the DTFM signal amplitude with respect to z_{min} is due to the large tip oscillation amplitude (10nm), with a change of only +/- 15% over a tip-sample gap range of +/- 0.5 nm near the surface. In these measurements, the value of z_{min} is estimated to be the distance that the tip is pulled back from the minimum of the df-z curve. The uncertainty in this estimate is of the order of a few Angstroms. This uncertainty does not limit the comparison of the simulated and measured DTFM signal amplitude here.

Figure 3.6(c) shows the DTFM amplitude versus z_{min} as the tip height is ramped in the special case where electron shuttling number goes from zero to one to two as the

Figure 3.6 DTFM signal amplitude as a function of V_{ac} and z_{min}. (a) A comparison of the DTFM amplitude versus V_{ac} relationship between experimental data and simulated values. z_{min}=0.5nm. (b) A comparison of DTFM amplitude versus z_{min} relationship between experimental data and simulation, with V_{ac}=3V. States 1 to 5 in this figure correspond to the states numbered in Figure 3.5(a). States 2, 3, 4, and 5 involve only single electron tunneling. State 1 involves two electron shuttling. In (a) and (b), data points are measured from multiple DTFM images obtained at the same location of the surface at different V_{ac} and z_{min}. The mean value and standard deviation of the DTFM amplitude for a given state are calculated by measuring six line cuts across that state in an image. (c) DTFM-z_{min} curve acquired by a tip height ramp at a location in which two trap states exist, with V_{ac} = 4V. Blue and green curves are experimental data acquired from forward and backward height ramps. A background offset when no electron shuttling occurs has been subtracted from the experimental data.

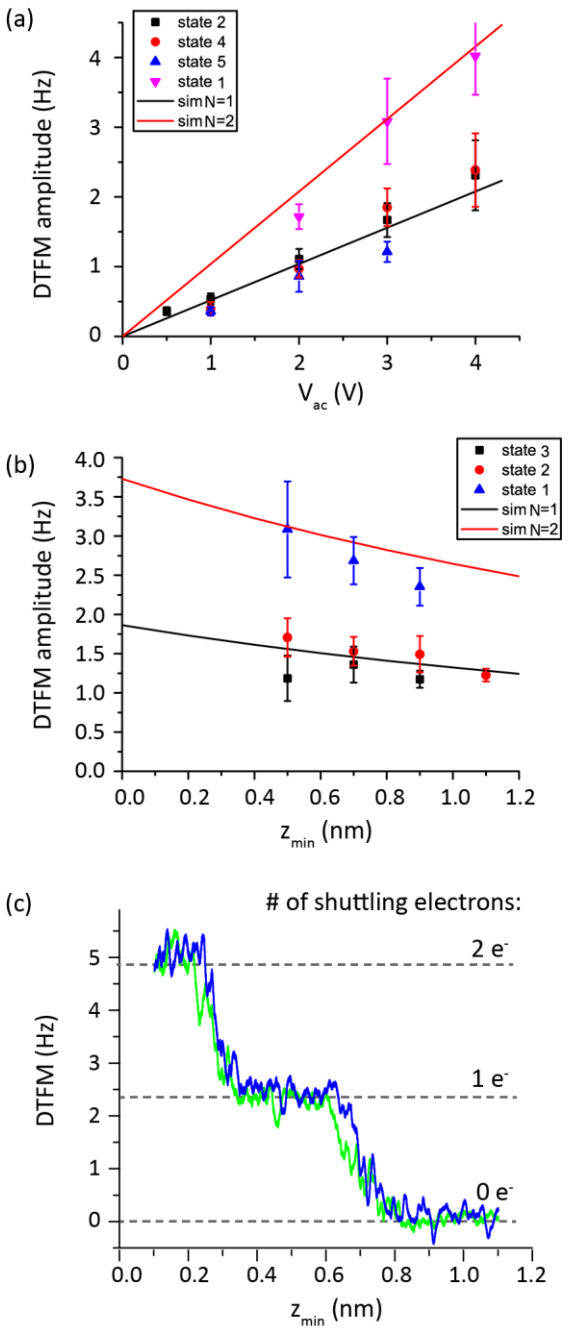
(a)
state 2
state 4
state 5
state 1
sim N=1
sim N=2
DTFM amplitude (Hz)
V_ac (V)
(b)
state 3
state 2
state 1
sim N=1
sim N=2
DTFM amplitude (Hz)
z_min (nm)
(c)
# of shuttling electrons:
2 e-
1 e-
0 e-
DTFM (Hz)
z_min (nm)

tip gets close to the surface. This is explained by the existence of two trap states under the tip at slightly different depths. As the tip approaches the surface, one state initially comes into tunneling range and then the second one. The approximately equal size of the two steps of the DTFM amplitude is consistent with the proportional relationship between DTFM amplitudes and shuttling electron number predicated by the theory. The quantized DTFM amplitude confirms again the single electron tunneling picture. Note that the DTFM amplitude sharply rises between zero, one and two electron shuttling plateaus. The sharp transition of DTFM amplitudes with tip heights (width~0.1nm) is consistent with the exponential dependency of tunneling rate with tunneling gap.

3.6 Conclusion

DTFM is a powerful technique for characterizing trap states in dielectric films on an atomic scale. The physical basis for DTFM measurements is explained and illustrated through a derivation of the DTFM signal, based upon a one-dimensional electrostatic model. Experimental data provide support to this dynamic single electron tunneling model. DTFM signal amplitudes from the experiment demonstrate quantitative consistency with theoretically simulated values. DTFM signal amplitude dependence on experimental parameters such as shuttling electron number, applied AC voltage, and probe tip height are also verified by the experiment.

3.7 References

[1] J. P. Johnson, N. Zheng, and C. C. Williams, Nanotechnology 20, 055701 (2009).

[2] R. Wang, S. W. King, and C. C. Williams, Appl. Phys. Lett. 105, 052903 (2014).

[3] J. P. Johnson, D. W. Winslow, and C. C. Williams, Appl. Phys. Lett. 98, 052902 (2011).

[4] T. A. Pomorski, B. C. Bittel, P. M. Lenahan, E. Mays, C. Ege, J. Bielefeld, D. Michalak and S. W. King, J. Appl. Phys. 115, 234508 (2014).

[5] T. A. Pomorski, B. C. Bittel, C. J. Cochrane, P. M. Lenahan, J. Bielefeld, and S. W. King, J. Appl. Phys. 114, 074501 (2013).

[6] J. M. Atkin, E. Cartier, T. M. Shaw, R. B. Laibowitz, and T. F. Heinz, Appl. Phys. Lett. 93, 122902 (2008).

[7] M. E. Welland and R. H. Koch, Appl. Phys. Lett. 48, 724 (1986).

[8] T. Ruskell, R. Workman, D. Chen, D. Sarid, S. Dahl, and S. Gilbert, Appl. Phys. Lett. 68, 93 (1996).

[9] B. Kaczer, Z. Meng, and J. P. Plez, Phys. Rev. Lett. 77, 91 (1996).

[10] R. Ludeke and E. Cartier, Appl. Phys. Lett. 78, 3998 (2001).

[11] S. Morita, M. Abe, K. Yokoyama, and Y. Sugawara, J. Cryst. Growth 210, 408 (2000).

[12] Y. Naitou, H. Arimura, N. Kitano, S. Horie, T. Minami, M. Kosuda, H. Ogiso, T. Hosoi, T. Shimura, and H. Watanabe, Appl. Phys. Lett. 92, 012112 (2008).

[13] L. J. Klein and C. C. Williams, Appl. Phys. Lett. 81, 4589(2002).

[14] E. Bussmann, D. J. Kim, and C. C. Williams, Appl. Phys. Lett. 85, 2538 (2004).

[15] E. Bussmann, and C. C. Williams, Appl. Phys. Lett. 88, 263108 (2006).

[16] A. Dana and Y. Yamamoto, Nanotechnology 16, S125 (2005).

[17] R. Stomp, Y. Miyahara, S. Schaer, Q. Sun, H. Guo, P. Grutter, S. Studenikin, P. Poole, and A. Sachrajda, Phys. Rev. Lett. 94, 056802 (2005).

[18] E. Bussmann, Ph. D. (2006). *Single electron tunneling force microscopy.* Doctoral dissertation, University of Utah.

[19] Nanoelectronics and Information Technology: Advanced Electronic Materials and Novel Devices, edited by R. Waser (John Wiley & Sons, New York, 2003), Chap. 16.

[20] F. J. Giessibl, Appl. Phys. Lett. 78, 123 (2001).

[21] N. Zheng, C. C. Williams, E. G. Mishchenko, and E. Bussmann, J. Appl. Phys. 101, 093702 (2007).

[22] E. Bussmann, N. Zheng, and C. C. Williams, Appl. Phys. Lett. 86, 163109 (2005).

[23] W. Melitz, J. Shen, A. C. Kummel, and S. Lee, Surf. Sci. Rep. 66, 1 (2011).

[24] S. King, B. French, and E. Mays, J. Appl. Phys. 113, 44109 (2013).

[25] Z. -Y. Lu, C. J. Nicklaw, D. M. Fleetwood, R. D. Schrimpf, and S. T. Pantelides, Phys. Rev. Lett. 89, 285505 (2002).

[26] S. W. King, M. French, M. Jaehnig, M. Kuhn, and B. French, Appl. Phys. Lett. 99, 202903 (2011).

CHAPTER 4

ENERGY AND DEPTH DETERMINATION OF INDIVIDUAL ELECTRONIC TRAP STATES

In this chapter, energy and depth determination of individual electronic trap states is illustrated. The physical tunneling model is presented and previous methods developed in the Williams' group for measuring state energy and depth are reviewed. A new method is demonstrated to eliminate the undesirable ambiguity in the energy/depth determination by that method used in Chapter 2. The possibility of extracting the state depth from DTFM amplitude is also discussed at the end of this chapter.

4.1 Tunneling Model Used for Determining State Energy and Depth

There are several papers from the Williams' group which discuss the measurement of the energy of an individual electronic trap state on a nonconducting surface [1-5]. Those methods are all based on a similar physical model of electron tunneling as illustrated in Figure 4.1(a). When a metallic AFM tip is brought close to an electronic trap state on dielectric surface, the depth of the state accessible to tunneling from the tip is determined by the tunneling barrier, which includes the barrier in the gap and in the film. The barrier height is a function of the trap state energy. With the band structure of the tip and dielectric known, the elastic tunneling rate (W) between a state

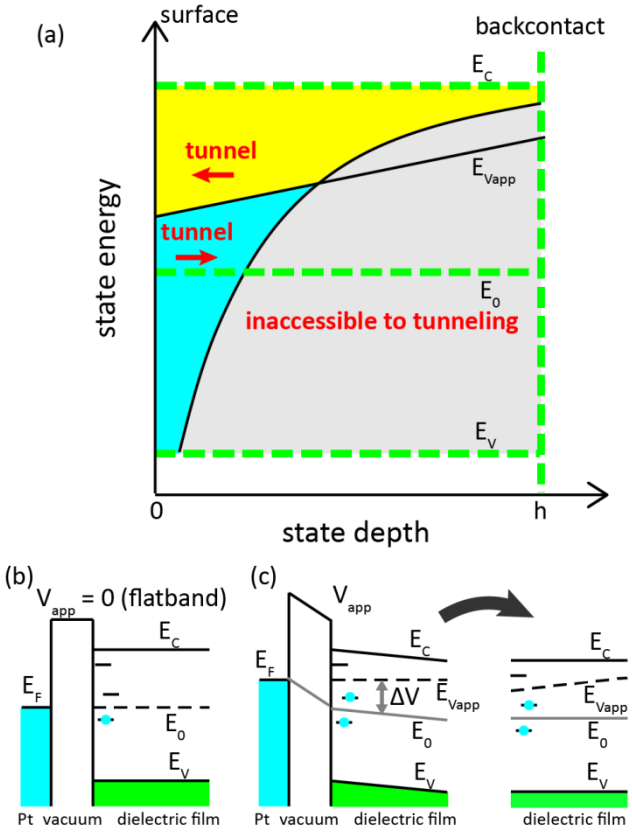

Figure 4.1 Tunneling and electrostatic models. (a) An illustration of tunneling model. E_C, E_V, E_0, E_{Vapp}, and h denote the energy of the conduction band, valence band, tip Fermi energy at flat band condition, tip Fermi energy at an applied voltage between tip and the sample back-contact V_{app}, and film thickness. At applied voltage V_{app}, the yellow region is where the electron can tunnel from a filled state to the tip, cyan region is where electron can tunnel from the tip to an empty state, and gray region is where tunneling is forbidden. The energy diagram of the tip and dielectric system at flat band condition is show in (b) and at a bias voltage V_{app} is shown in (c). In (c), ΔV is the voltage drop between the tip and a state at a given depth.

with energy (E) and depth (d) and a tip at tip/surface gap (z) can be calculated [2]. For experimental measurement time Δt, the contour of

$$\mathrm{W(E,d,z)} = \frac{1}{\Delta t} \tag{4.1}$$

is a curve in energy/depth space which divides the regions accessible and inaccessible to tunneling (see Figure 4.1(a)) in that measurement time. The shape of the curve in the figure indicates that tunneling electrons can reach deeper states for smaller energy barrier.

The second consideration in this tunneling picture is the relative energy levels of the tip Fermi level and the electronic state. As stated previously, an empty state in the dielectric surface below Fermi level of the tip gets filled by electron tunneling from the tip and a filled state above Fermi energy of the tip gets emptied as electron tunnels from that state to the tip. Figure 4.1 (b) and (c) show energy diagrams of the tip and dielectric system at flat band condition and at an applied voltage. The voltage drop between tip and a state at a depth d is:

$$E_{Vapp} = \Delta V = V_{app}\,\frac{z + \frac{d}{k}}{z + \frac{h}{k}}, \tag{4.2}$$

with h and k representing the thickness and the dielectric constant of the dielectric film.

4.2 Review of Energy and Depth Measurements

Several previous energy measurement papers are based on the simple tunneling model described above. In Reference [1], during a voltage scan, when the E_{Vapp} line in Figure 4.1(a) goes across the energy of an existing state, the state changes its occupation status due to tunneling. This change leads to a sudden change of df in the otherwise

smooth df-V curve. The voltage value at which this change occurs was used to calculate back the state energy using equation (4.2). In order for the tunneling to occur immediately after the voltage is swept across the transition value, the tunneling probability needs to be high for a given experimental time related to the voltage scanning speed. Violation of this requirement will lead to a hysteresis as shown below. In that work, the state depth is assumed to be zero and therefore, no depth information is extracted.

Another way of detecting electron tunneling is to measure surface potential change after tunneling occurs, with a methodology of KPFM [6] by applying a voltage modulation. The applied voltage at which a tunneling event occurs is again used to calculate the state energy in those previous papers [2-5].

In order to extract state depth information as well as state energy, Reference [5] presents a methodology by varying both applied voltage and tip height. A set of voltage and tip height values are used. It is equivalent to moving both the constant tunneling probability contour curve and the E_{Vapp} line in Figure 4.1(a) to divide the energy/depth space into separate differential sections. In this method, electronic state energy and depth are therefore measured to be in one of these differential energy/depth regions by differential subtraction.

Inspired by the method in Reference [5], work in Chapter 2 of this thesis shows the acquisition of DTFM images at a set of different AC voltage amplitudes and tip heights. Energy and depth of a specific state is extracted based on the voltage and tip height values at which this state appears in the DTFM images acquired, using a similar tunneling and electrostatic model.

4.3 A Method to Eliminate the Ambiguity in Energy/Depth Measurements

This section describes a method to determine the energy/depth of a specific state without the ambiguity of resulting in two separate energy/depth regions associated with varying the AC voltage as described in Chapter 2.

A DTFM image is first acquired to provide a 2D map of trap states. Locating the tip above a specific state, a df-V curve and a DTFM-z_{min} curve are taken. The voltage and z_{min} values at which tunneling is observed in the two curves are then used to extract the energy and depth of that state. Compared to using a discrete set of voltage and tip height values at each point, continuous scans determine the energy and depth exactly (within experimental errors) rather than within a region of energy / depth space.

Before demonstrating this methodology to measure 3D location and energy of a state, a detour is made to inspect df-V curves behavior as a function of tip heights. This exploration provides further evidence for the tunneling and electrostatic models used to extract state energy and depth. It also guides experiment in acquiring df-V curve at a proper tip height.

During the voltage scan in acquisition of a df-V curve at a fixed tip height, tunneling will occur immediately after the energy condition is met only if the tunneling rate is fast compared to the voltage scan rate. The voltage values at which the tunneling occurs should be the same irrespective of the direction of the voltage scan, and the voltage value at which the tunneling occurs (call it V_{tr}) is used to extract state energy and depth. But when the tip is farther from the surface, the tunneling rate is lower, in which case a delay could occur between the time the tip Fermi level goes across the state energy

level and the tunneling event. Figure 4.2 shows df-V curves taken at different tip heights above a particular state in a 10nm SiO_2 film. For each curve, 2000 data points are recorded with 5ms between every two data points as the voltage is ramped from 0V to 4V and then from 4V to 0V. No tunneling occurs in the curve acquired at a high of 1.5 nm (z=1.5 nm) because the tunneling rate is too small to be detected. For z=1.4nm, the tunneling rate is faster, but is still slow compared to voltage scanning rate; therefore, a delay occurs as predicted, causing a hysteresis between forward and backward voltage ramps (from 0V to 4V or from 4V to 0V). From z=1.4nm to z=1.2nm, the delay and the hysteresis become smaller because of increase of the tunneling rate. Between z=1.1nm and z=0.9nm, the hysteresis disappears and a telegraph signal is observed caused by sporadic tunneling of an electron back and forth between the probe and sample around the transition voltage value, with a telegraph width on the order of 0.5V. The ~0.5 V width of the transition region corresponds to an energy range of ~0.15 eV. Explanations for this transition width are not clear. The telegraph signal frequency is controlled by the tunneling rate and increases as the tip goes closer to the surface. At z=0.8nm and z=0.6nm, telegraph signal frequency gets high enough to be filtered out by the finite bandwidth of the frequency shift measurement, and becomes a slowly changing slope in the curves. Other features seen in Figure 4.2 are also consistent with the single electron tunneling model. For example, V_{tr} increases as tip height decreases because of the decrease of voltage drop between tip and the state, and the df step due to single electron tunneling is larger at higher voltage because of the larger electrostatic force change at higher applied voltages. In order to accurately extract V_{tr}, the df-V curve should be acquired at a tip height which is not too large to avoid hysteresis, and not too small to

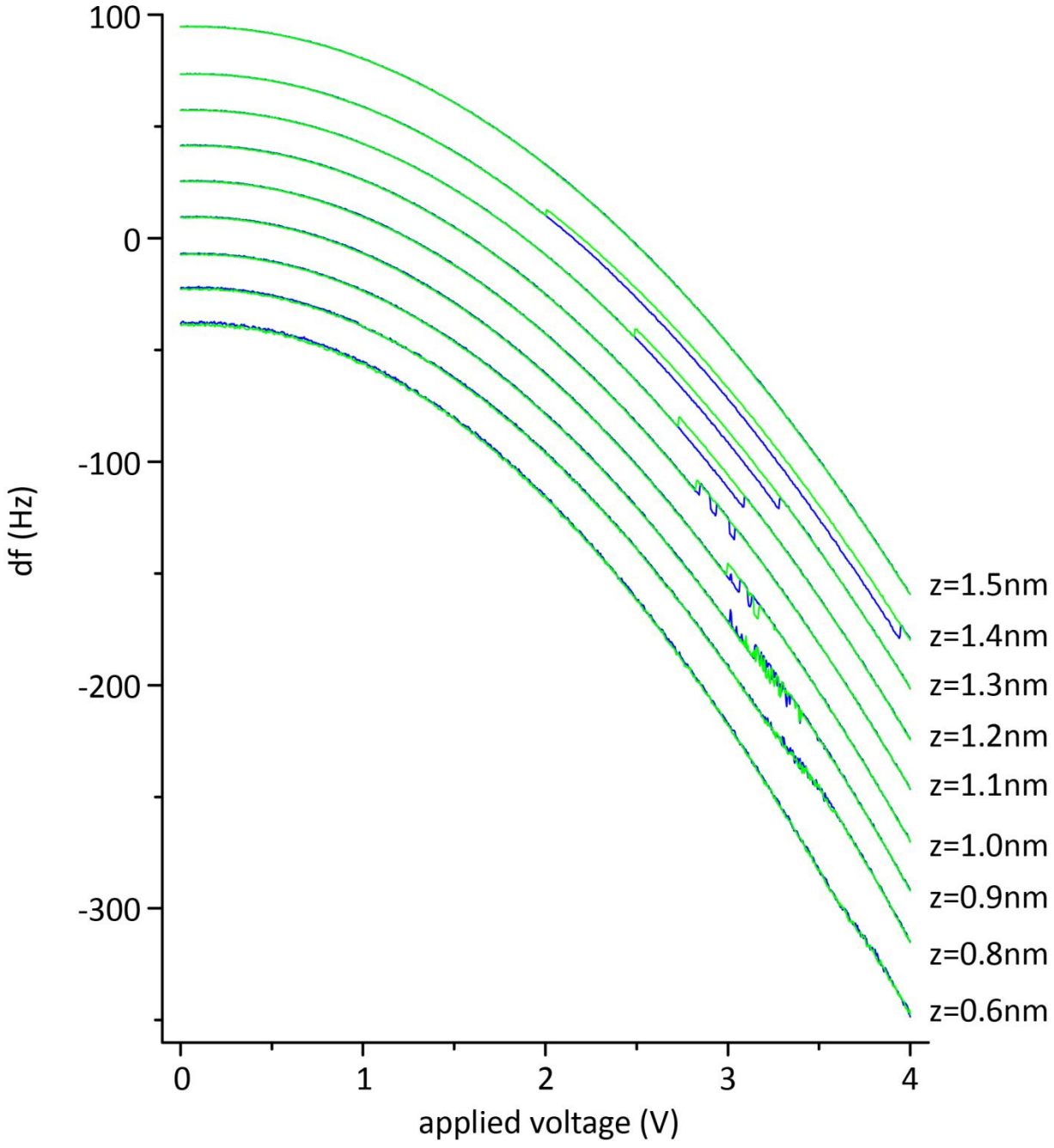

Figure 4.2 df-V curves taken above a trap state in a 10nm SiO_2 film at different tip heights (z). Voltage is ramped forward (from 0V to 4V) in blue curves, and backward (from 4V to 0V) in green curves. The curves are shifted vertically with respect to each other for clear visualization.

avoid a slow transition due to filtering.

The 3D location and energy determination of a single state is demonstrated in Figure 4.3 by acquiring a DTFM image, a df-V curve, and a DTFM-z_{min} curve. The DTFM image is first taken and a specific state with a known 2D location is chosen as marked by the blue spot in Figure 4.3(a). In Figure 4.3 (b), the df-V curve is shown acquired at z=0.8nm with a transition voltage V_{tr} centered at 1.7V with a full spreading width of 0.3V. Based on the model discussed in section 4.1, this state locates on a line in energy (E) and depth (d) space defined by equation (4.2) with V_{app}=1.7V and z=0.8nm. This is the red line drawn in Figure 4.4. In the DTFM-z_{min} curve in Figure 4.3 (c), DTFM signal rises when the tunneling rate increases to ~300Hz (DTFM AC voltage frequency) at 0.6nm. The state locates on the curve defined by $W(E,d,z) = 1/f_{Vac}$, with f_{Vac}=300Hz, and z=0.6nm. This curve is the blue curve shown in Figure 4.4. The intersection of the line and the curve in Figure 4.4 is the energy and depth solution for the state: the state energy is 0.57eV and depth is 1.1nm. Relevant physical parameters used in calculation are: electron effective mass is 0.5 times vacuum electron mass [7], platinum tip work function is 5.4eV [8], platinum tip Fermi energy relative to bottom of band is 8.5eV, electron affinity of SiO_2 is 0.9eV [9], relative dielectric constant of SiO_2 is 4.2 [10], and SiO_2 band gap is 8.8eV [10]. Zero energy in Figure 4.4 is again defined as the tip Fermi level at the flat band condition, corresponding to 4.3eV above valence band edge of SiO_2. Thus, the measurement of 3D spatial location and energy of an individual state is demonstrated.

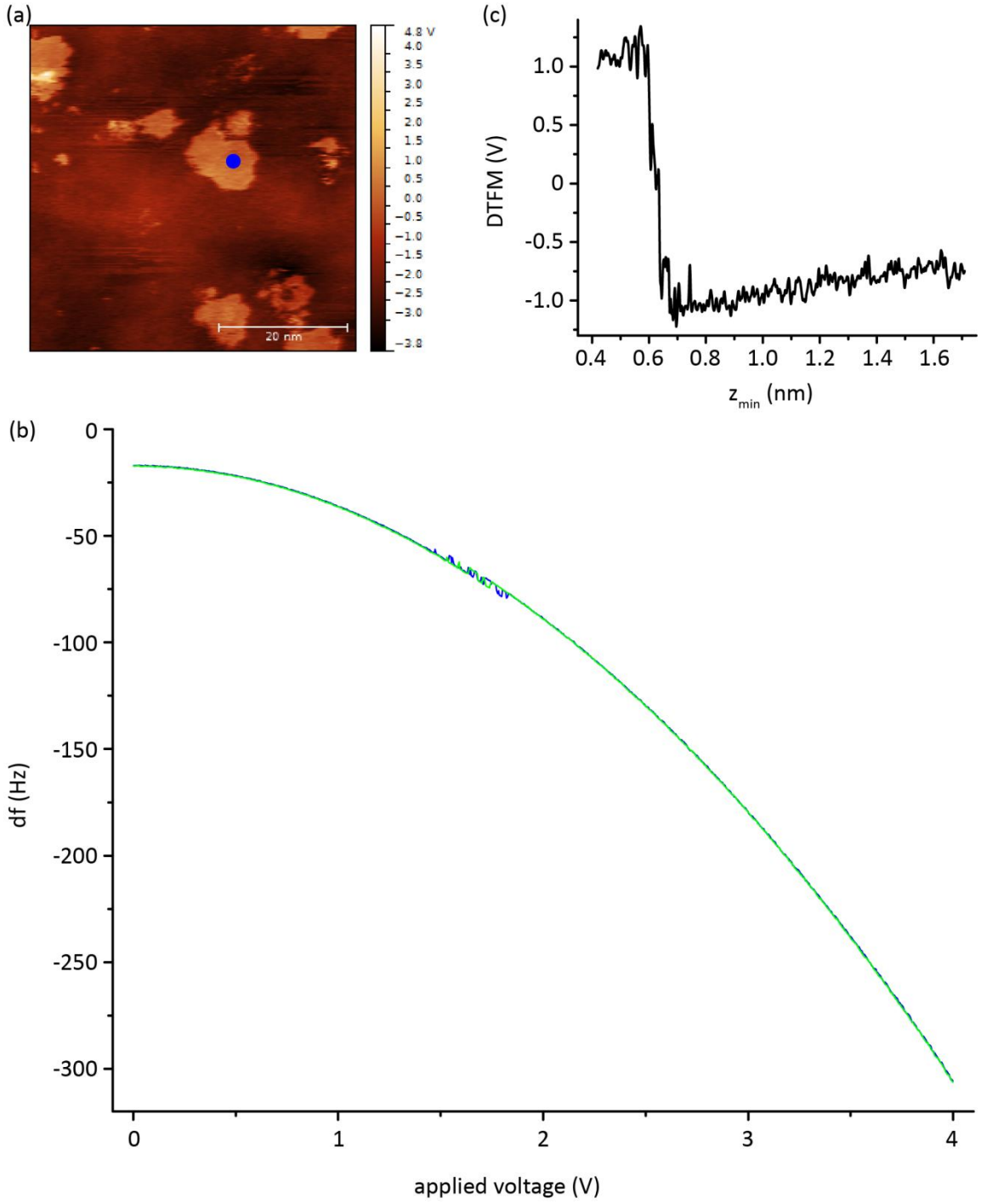

Figure 4.3 Measurement of 3D location and energy of a trap state. (a) A DTFM image taken on a 10nm SiO_2 surface with V_{ac}=4V, z_{min}=0.2nm. The df-V curve in (b) and DTFM-z curve in (c) are taken at the location of the blue spot. (b) df-V curve is taken at tip height z=0.8nm, while voltage is scanning from 0V to 4V (blue) and from 4V to 0V (green). (c) DTFM-z_{min} curve is taken with V_{ac}=4V.

4.4 DTFM Signal Amplitude as a Function of State Depth

From the simplified parallel plate model of the tip and surface system, equation (3.8) shows the DTFM amplitude is linearly dependent on the distance between the trap state and sample back-contact (h-d). This could, in principle, be used to extract the state depth from the DTFM amplitude. In Figure 4.5, data points correspond to all the states observed in the image shown in Figure 3.5(a). The mean value and standard deviation of DTFM amplitude of each state is measured by taking six line cuts across that state, as previously described. The depth of each state is obtained from the measurement result in Figure 2.4 by differentially subtracting energy/depth regions of DTFM images at different V_{ac} and z_{min} values. The theoretical result, of the DTFM amplitude as a function of state depth d according to equation (3.7), is shown by the red line in the Figure 4.5. The correlation between the experimental data and the theory is not definitive because of the weak dependency of DTFM amplitude on state depth in the theory and the large uncertainty in both state depth and DTFM amplitude in the experimental data.

4.5 References

[1] E. Bussmann, and C. C. Williams, Appl. Phys. Lett. 88, 263108 (2006).

[2] N. Zheng, J. P. Johnson, C. C. Williams, and G. Wang, Nanotechnology 21, 295708 (2010).

[3] W. Winslow, J. P. Johnson, and C. C. Williams, Appl. Phys. Lett. 98, 172903 (2011).

[4] D. Winslow and C. Williams, J. Appl. Phys. 110, 114102 (2011).

[5] J. P. Johnson, D. W. Winslow, and C. C. Williams, Appl. Phys. Lett. 98, 052902 (2011).

[6] W. Melitz, J. Shen, A. C. Kummel, and S. Lee, Surf. Sci. Rep. 66, 1 (2011).

[7] J. Borja, J. L. Plawsky, T. M. Lu, H. Bakhru and W. N. Gill, J. Appl. Phys. 115, 084107 (2014).

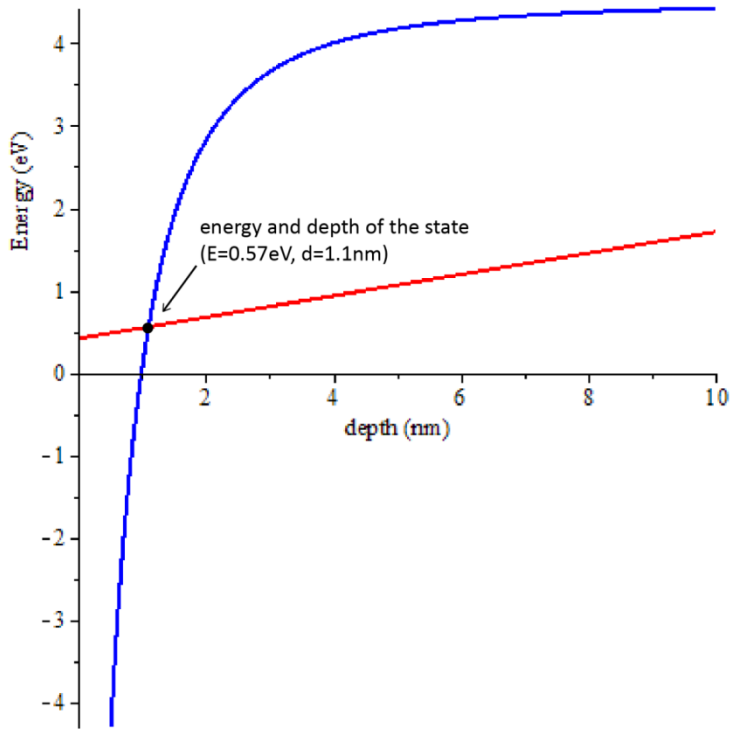

Figure 4.4 Determination of energy and depth of the state from Figure4.3.

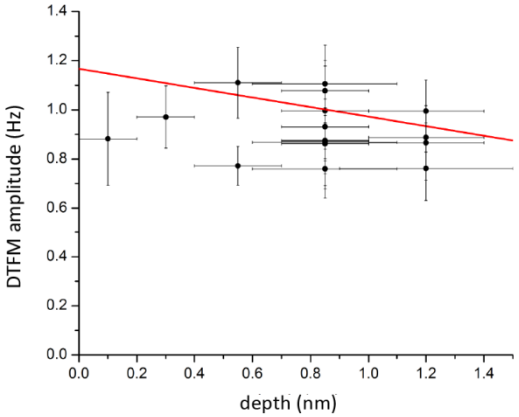

Figure 4.5 Comparison between experimental and simulated DTFM amplitude vs. state depth relationships. Data points show the measured DTFM depths and DTFM amplitudes for all states in Figure 3.5(a). The red line shows the DTFM amplitude as a function of state depth calculated by the theory.

[8] Chanhyung Kim, Journal of the Korean Physical Society, Vol. 47, November 2005, pp417.

[9] S. D. Brorson, D. J. DiMaria, M. V. Fischetti, F. L. Pesavento, P. M. Solomon, and D. W. Dong, J. Appl. Phys. 58, 1302 (1985).

[10] S. King, B. French, and E. Mays, J. Appl. Phys. 113, 44109 (2013).

CHAPTER 5

ATOMIC SCALE STUDY OF ELECTRICAL STRESS EFFECT ON LOW-K DIELECTRIC FILM USING DYNAMIC TUNNELING FORCE MICROSCOPY

An important motivation of the characterization of defect states in low-k materials is to study the electrical reliability of those materials. Local current leakage can be measured by the conductive-AFM (c-AFM) method. Comparison of c-AFM and DTFM images taken on the same location of the surface may illuminate the correlation between trap states measured by DTFM and defect states participating in conduction. Another important topic on electrical reliability is the electrical stressing effect. AFM provides a microscopic tool for studying electrical stressing effects at an atomic scale level. Local electrical stressing is applied by a voltage biased AFM tip on a dielectric surface, and the DTFM images are acquired at the same location before and after the stressing to observe any change in local states due to electrical stress.

A 6nm low-k interlayer dielectric film (k=3.3) $SiO_{1.2}C_{0.35}$:H fabricated by researchers at Intel Corporation is used in this study. Details concerning the film deposition processes can be found in Refence [1]. The samples were ultrasonically cleaned both in acetone and isopropyl alcohol for 15 minutes, then rinsed in deionized water and blown dry with nitrogen gas. The samples were then inserted in the UHV chamber and heated at 380°C for 1 hour to desorb water and organic contaminants

resulting from the ambient exposure.

5.1 Correlation between Trap States Measured by DTFM and High Conductivity Locations Measured by C-AFM

One objective of studying trap states using DTFM is to explore the role those states play in film leakage. High conductivity (leakage) locations of the film can be imaged by c-AFM, in which the metallic AFM tip acts as a moving electrode while a voltage is applied between the tip and the back-contact of the dielectric film. The current through the film is collected as a function of surface location during imaging. By comparing trap state locations measured by DTFM and high conductivity locations measured by conductive-AFM on the same area of a dielectric surface, we can find out whether the two are correlated.

Figure 5.1 shows the DTFM image and c-AFM images taken in the same surface area on the sample. We can see that the correlation between the trap states measured by the DTFM image and high conductivity locations measured by conductive-AFM images is weak. However, this observation does not necessarily lead to the conclusion that the conductivity of this film is not caused by or related to trap states. If we assume the high conductivity locations detected by c-AFM are caused by defect states near the conduction band, those states are not likely to be detected by DTFM for the following reasons.

First, the detection window of a DTFM experiment in energy and depth space is determined by experimental parameters of V_{ac} and z_{min}. Figure 5.1 (d) shows the energy/depth window detected by the DTFM experiment in Figure 5.1 (b) calculated using the method discussed in Chapter 2. The dielectric film electron affinity of this dielectric material is 0.7eV [4] and band gap is 8.2eV [1]. It is seen that only a small

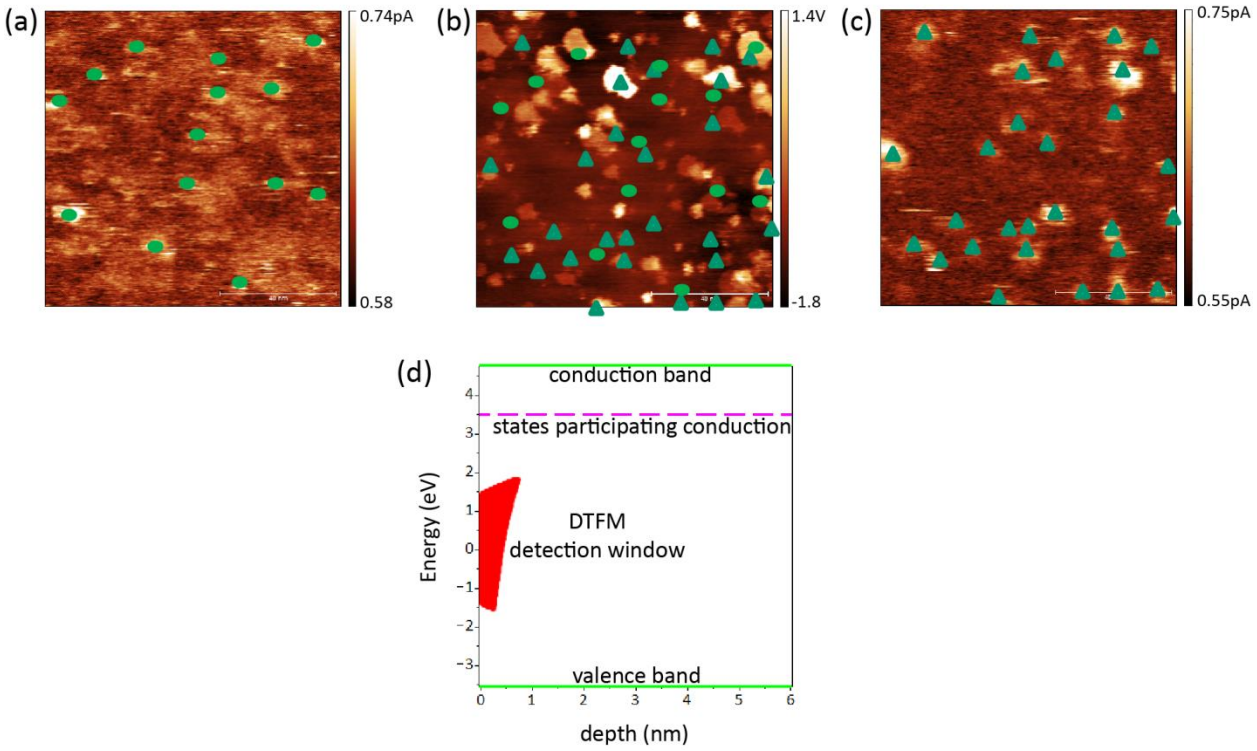

Figure 5.1 Comparison between DTFM and c-AFM images. Images (a), (b), and (c) are acquired in the same area of a 6nm low-k ILD film (k=3.3) $SiO_{1.2}C_{0.35}$:H sample. (a) and (c) are current images with applied voltages of 8V and -6V applied to the sample back-contact respectively with tip grounded. (b) is a DTFM image with V_{ac}=5V, z_{min}=0.7nm. To facilitate comparison between images, high current locations are marked with ovals and triangles respectively in (a) and (c) and overlaid on (b). (d) is the energy/depth space of trap states. The red region shows the energy and depth of states accessible by DTFM experiment in (b). The dashed line is the energy above which trap states likely participate in conduction from Reference [2] and [3].

portion of the whole available energy/depth space – with energy between conduction band and valence band and with depth between zero and the film thickness -- are accessible by DTFM. Even though this detection window can be enlarged by increasing V_{ac} and decreasing z_{min}, due to experimental considerations such as breakdown, surface charging, and stability of AFM scanning, the detection window shown in Figure 5.1 (d) is approximately the maximum detection window for DTFM experiment on this particular sample. The energy of the states accessible by DTFM is shown to locate between 3eV and 6eV below the conduction band edge of this material. In samples similar to the one used in this experiment, trap states have been found to contribute to film conductivity [2,3]. Energy levels of the trap states which cause film leakage can be extracted by fitting current-voltage data to conduction mechanisms. Atkin et al. reported the effective barrier height of trap states participating in Poole-Frenkel emission is 1.2eV [2]. Gischia et al. measured Fowler-Nordheim tunneling trap barrier height is ~1.1eV [3]. The energy levels of those states participating film conduction are much higher than states measured by DTFM (see Figure 5.1(d) the red region compared to the dashed line). In another words, the states dominating conduction have energies much closer to the conduction band, compared to the states measured by DTFM.

Second, DTFM can only detect trap states with a finite electron dwelling time, which is determined by the shuttling voltage (V_{ac}) frequency. V_{ac} used in this work is at ~300Hz frequency. In order for an electron to shuttle between the tip and the trap state at that frequency, the state has to be able to hold the electron, without leaking away, for about 1.5ms. If a conductance measurement were performed through such a state, the maximum current would be approximately 100 atto-amperes. On the other hand, the

threshold of detectable current in c-AFM experiment is on the order of 100fA, which is determined by sensitivity of the current amplifier used (Femto current amplifier DLPCA-200). This threshold current amplitude corresponds to ~10^6 electrons/second. So, an electron must spend less than 1μs at a given defect state before leaking away in order to contribute to a detectable current. The electron dwelling times of states measured by c-AFM and DTFM do not overlap.

Therefore, DTFM and c-AFM are accessing states at different energy levels and with different electron dwelling times. In order for DTFM to be used to characterize states related to film leakage, two modifications of DTFM are proposed for future experiment. First, in order for DTFM to access states of energy near the conduction band, the tip Fermi level should move closer to the energy level of states to be detected. This can be realized by choosing tips of different metal materials and therefore of different work functions. Second, to access faster or leakier states, DTFM needs to use a shuttling voltage V_{ac} of higher frequency. If the current method is simply extended to higher frequency, it may be limited by the PLL bandwidth, which is on the order of 100kHz. Other approaches are currently being considered to overcome this limitation.

5.2 Atomic Scale Study of Electrical Stress Effect on Local States

Two experiments are conducted to observe trap state changes after applying a local electrical stress to the surface using AFM probe tip. Electrical stressing is applied by fixing a voltage biased AFM tip at a certain location in the first experiment and by scanning a voltage biased AFM tip over an area in the second experiment.

In the experiment corresponding to Figure 5.2, a DTFM image is first acquired on

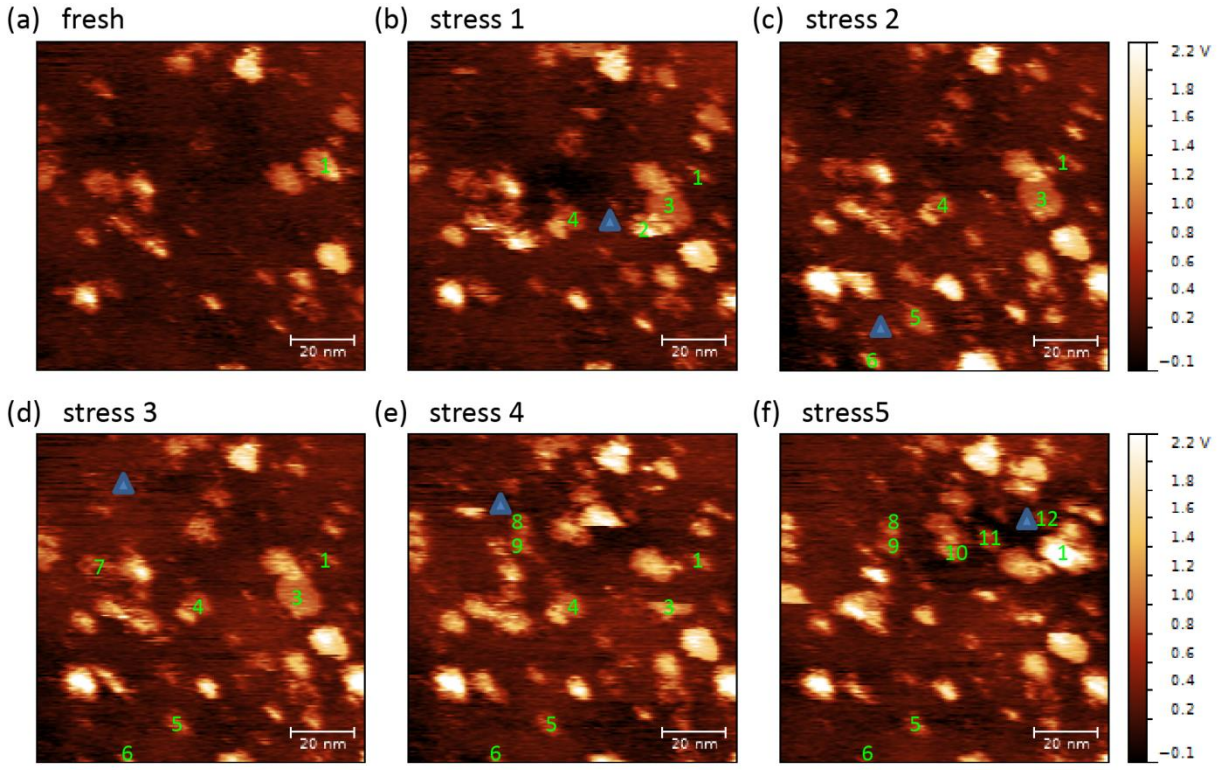

Figure 5.2 DTFM images obtained on a k=3.3 ILD film in between a series of point electrical stresses. (a) is a DTFM image taken before any electrical stress has been applied. (b),(c),(d),(e), and (f) are DTFM images taken after electrical stresses 1-5 have been applied at the locations marked by the blue triangles. For each stress, 9V is applied to the sample back-contact for 1 minute with the tip grounded. The DTFM imaging parameters are V_{ac}= 5V and z_{min}=0.5nm. Twelve specific electronic states are numbered in green in the images for reference later. States by the same number in different images are the same trap state identified by its location.

a fresh $(100nm)^2$ area of the sample surface before any electrical stress is applied. A point electrical stress is then applied by parking the AFM tip at a location for 1 minute with a voltage of 9V applied to the sample back-contact with the tip grounded (electrical field is 15MV/cm). Notice the location of the stress is intentionally chosen at a location where no trap states are originally observed. After the electrical stress, DTFM images are taken in the same surface area to look for any change in the observable trap states. The electrical stressing experiment is then repeated at different locations, each time followed by DTFM imaging. The blue triangles indicate the locations of the probe tip where electrical stress is applied. The DTFM images shown in Figure 5.2 are taken in time order. To be more specific, image (a) is taken first, and then stress 1 is applied, and then image (b) is taken, and then stress 2 is applied, etc.

Before performing this electrical stressing experiment in Figure 5.2, DTFM images are taken repeatedly in this same area with the same parameters as used in Figure 5.2. The trap states are observed to repeat well in DTFM images without the additional stress (data not shown). After the electrical stress is applied, we observe new states appearing and also some previously existing states disappearing. The modification of states is observed only in locations near the electrically stressed point (within ~30 nm radius). Trap states away from the stressed region stay largely unchanged. Table 5.1 summarizes the observations of state appearance and disappearance shown in Figure 5.2. We can see that out of five trials with an electrical stress of 15MV/cm for 1 minute at different locations, there is only one stressing event after which no trap states either appear or disappear. The average number of states created per electrical stressing event is two. In this set of measurements, only one state disappears, as compared to ten which

Table 5.1 Specific states (by their number identified in Figure 5.2) which appear or disappear in the experiment in Figure 5.2.

stresses	States appearing (by state number)	States disappearing (by state number)
1	#2,#3,#4	none
2	#5,#6	none
3	none	none
4	#8,#9	#7
5	#10,#11,#12	none

appear. However, the ratio of the number of states appearing and disappearing in this experiment is not a fair comparison, as electrical stressing was intentionally applied in locations where few trap states pre-existed. The areal stressing experiment described below will provide more reliable information on the ratio between appearance and disappearance of trap states due to electrical stress.

The electrical stressing effects could be due to either the electric field strength or the current effect. We currently do not have any evidence for the cause of state modification after electrical stressing.

We also observe that some states change apparent size in the DTFM image after electrical stress. For example, in Figure 5.2, state 1 becomes smaller in size after the first electrical stressing event. It then remains approximately the same apparent size until electrical stressing event 5, after which its apparent size becomes larger in the DTFM image. A change in the apparent size of a state in a DTFM image could be interpreted as change in depth or energy of the state or it may be just due to the elimination of one bond and creation of another.

Similar experiments have also been performed on the same sample with electrical stress at different polarities and electrical field strength. We observe that in 11 stressing events at different locations with +9V (15MV/cm) applied to the sample back-contact for 1 minute, 8 of the 11 stresses produced new states in DTFM images. In 8 stresses at a negative applied voltage of -8V (-13MV/cm) for 1 minute, 4 new states appeared in the DTFM images. These observations confirm that states can be created at different locations and at both positive and negative electrical field polarities.

As mentioned above, electrical stress is observed to affect states in an area of ~30

nm radius from the location where the stress is applied. The reason could be the finite radius of the metallic AFM probe tip, which is typically 20-35 nm for the Nanosensor PPP-NCHPt AFM probe tip we used. All locations under the tip apex are stressed even though the electrical field intensity is not expected to be uniform, depending on the geometry of the tip apex.

Since the film imaged is an amorphous film with nonuniform atomic structure, it is likely some locations are more susceptible to modification under electrical stress. Areal electrical stressing experiment is used to observe change in trap states as a function of spatial location under uniform electrical stressing. In this experiment, electrical stressing is applied over an area uniformly by scanning a voltage biased AFM tip across that area.

In Figure 5.3, the electrical stress is applied uniformly to a $(50nm)^2$ area inside the blue square by scanning a voltage biased AFM tip in that area with a total imaging time of 15 minutes for every scanning cycle. Four electrical stress scans are made with positive 8V (13MV/cm) and negative -7V (12MV/cm) alternatively at the same region. After each stress, DTFM images are taken in a larger area containing the stressed area. All images in Figure 5.3 are taken in the same surface location. To be clear, image (a) is first taken, then stress 1 is applied, then image (b) is taken, then stress 2 is applied, etc. In the stressed area and its vicinity, changes in the observed trap states are summarized in Table 5.2. Some new states appear while some previously existing states disappear after the electrical stress. The number of trap states which appear and disappear are approximately even. Change in apparent state size is also observed, such as state 1. Most of the states far away from the electrically stressed region remain unchanged after electrical stressing.

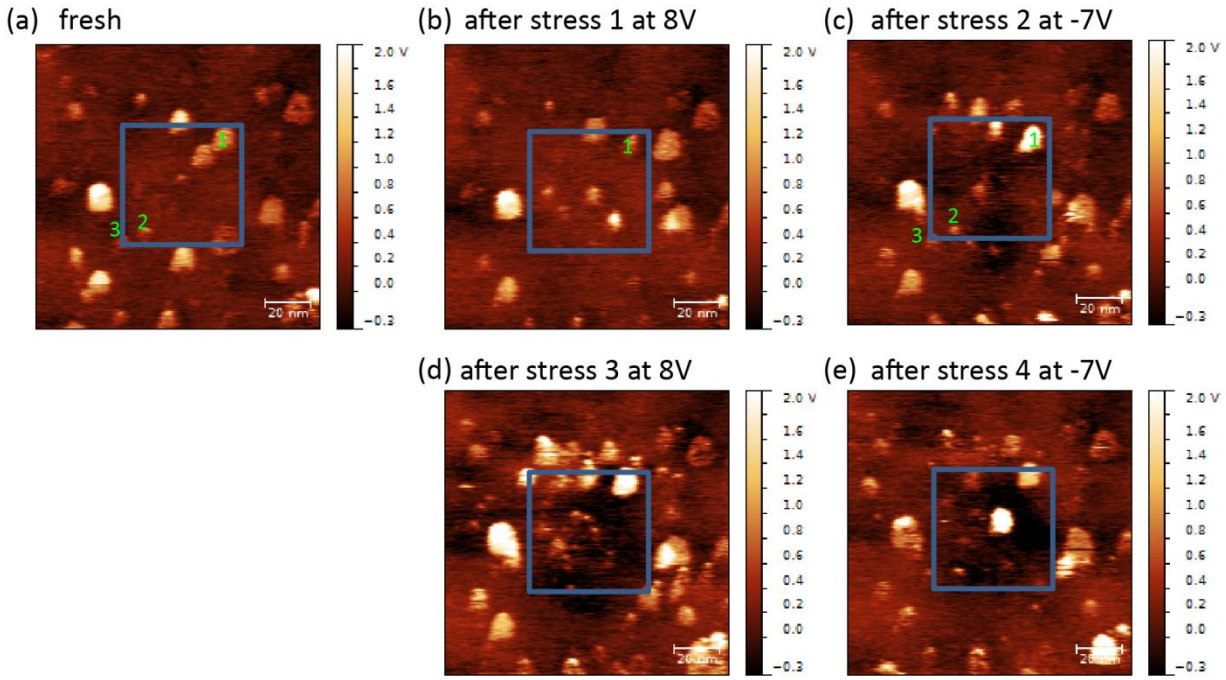

Figure 5.3 DTFM images measured on the same surface area when it is fresh and after each of four electrical stresses is applied in a smaller area inside that area. During stressing, a voltage of +8V (+13MV/cm) for stresses 1 and 3 or -7V (-12MV/cm) for stresses 2 and 4 is applied to the sample back-contact while the AFM tip is grounded. The AFM tip is scanned across a $(50nm)^2$ area inside the blue box to apply the stress. DTFM images are taken with V_{ac}= 5V and z_{min}=0.6nm. (a) DTFM image of the surface before electrical stress has been applied. (b),(c),(d),(e), and (f) are DTFM images taken after stresses 1-4 applied inside the blue square. Stresses 1, 2, and 3 were applied for one imaging cycle (15 minutes) and stress 4 was applied for three imaging cycles (45 minutes). Three states are marked in the images for future reference.

Table 5.2 The total number of states before and after each electrical stress in Figure 5.3 and the number of states which remain, appear, and disappear in the stressed area and its vicinity for each stress.

Stresses	Total No. of states before stressing	Total No. of states after stressing	No. of states unchanged	No. of new states appearing	No. of states disappearing
1	11	12	5	7	6
2	12	15	6	9	6
3	15	14	9	5	6
4	14	10	9	1	5

By applying positive and negative bias voltages alternatively, the effect of polarity is examined. The primary result is that states appear to change randomly after each stress is applied, regardless of its polarity.

Another observation from the experiment is that states created by electrical stress seem to be less stable than the original states which exist before the stressing. For example, the 1st stress created states 2, 3, and 4. State 2 disappears in the next DTFM image (Figure 5.3 (c)), and state 3 and 4 also disappeared in about an hour after their creation (Figure 5.3 (f)). In this specific case, all three states created by the electrical stress eventually disappeared.

In conclusion, electrical stress effects are studied on atomic scale using DTFM imaging. The observations show that trap states can appear or disappear due to local stressing. Further work is needed to verify and understand these effects.

5.3 References

[1] S. King, B. French, and E. Mays, J. Appl. Phys. 113, 44109 (2013).

[2] J. M. Atkin, T. M. Shaw, E. Liniger, R. B. Laibowitz, and T. F. Heinz, Reliability Physics Symposium (IRPS), 2012 IEEE International, pp. BD-1. IEEE, 2012.

[3] G. G. Gischia, K. Croes, G. Groeseneken, Z. Tokei, V. Afanas' ev, and L. Zhao, Reliability Physics Symposium (IRPS), 2010 IEEE International, pp. 549-555. IEEE, 2010.

[4] H. Zheng, S. W. King, V. Ryan, Y. Nishi and J. L. Shohet, Appl. Phys. Lett. 104, 062904 (2014).

CHAPTER 6

SUMMARY

The research in this thesis is focused on development and verification of a scanning probe microscopy method --Dynamic Tunneling Force Microscopy (DTFM) – for imaging and charactering individual atomic scale electronic trap states in non-conducting surfaces. This methodology is demonstrated in charactering defects in low-k dielectric thin film materials used in semiconductor devices.

DTFM is improved by experimentally introducing feedback loops of surface potential and resonance frequency shift, which enable simultaneous acquisition of two extra channels of information, surface potential and topography with the DTFM channel. Comparison between the three channels therefore will be available for studying correlation between trap state locations, local surface potential, and topography variations.

Energy and depth of electronic states are obtained through DTFM images at different AC voltage amplitudes and tip heights. A tunneling model is utilized to calculate the energy and depth of states accessed by a DTFM image. Therefore, 3D locations of states and energy of individual trap states can be extracted from DTFM experiments for the first time.

The DTFM method is based on a physics model of single electron tunneling between a metallic AFM tip and an isolated trap state in nonconducting surface. This model is verified by comparing the DTFM signal amplitude with experimental value.

With the power of imaging individual electronic trap states, DTFM is applied to monitor changes of trap states near the probe tip after application of a local electrical stress. Both defect state appearance and disappearance are observed within ~30nm radius of the stressing points. The cause for state modification due to electrical stressing needs further study.

States measured by DTFM are also compared to film leakage locations measured by c-AFM on a single dielectric film. The comparison shows that the two are not correlated. The likely reason is that DTFM measures states within a limited energy region and only on states with a slow electron leakage rate. In order to gain insight on states participating in film leakage, the DTFM method needs modification so that it can access states closer to the conduction band and states which have faster leakage rates. Further work is needed in this area.